ORNL/TM-2023/3122 Rev.1

Noble Gas Transport in the MSRE

Kyoung O. Lee
David Kropaczek
Aaron M. Graham

August 2023

Approved for public release.
Distribution is unlimited.

OAK RIDGE National Laboratory

ORNL IS MANAGED BY UT-BATTELLE LLC FOR THE US DEPARTMENT OF ENERGY

ORNL/TM-2023/3122 Rev.1

Nuclear Energy and Fuel Cycle Division

NOBLE GAS TRANSPORT IN THE MSRE

Kyoung O. Lee
David Kropaczek
Aaron M. Graham

August 2023

Prepared by
OAK RIDGE NATIONAL LABORATORY
Oak Ridge, TN 37831
managed by
UT-BATTELLE LLC
for the
US DEPARTMENT OF ENERGY
under contract DE-AC05-00OR22725

CONTENTS

LIST OF FIGURES

LIST OF TABLES

ABBREVIATIONS

NEAMS	Nuclear Energy Advanced Modeling and Simulation
MOOSE	Multiphysics Object Oriented Simulation Environment
MSR	molten salt reactor
MSRE	Molten Salt Reactor Experiment
ORNL	Oak Ridge National Laboratory

ABSTRACT

This study explores the relationship between the physicochemical parameter known as *Henry's gas constant* and gas transport across a two-layer film interface. The investigation utilized the Gibbs free energy, incorporating surface and volume terms to elucidate trends in enthalpy and entropy. Notably, our findings align with experimental data and offer predictive insights into the Henry's gas constants for helium and krypton, which hold significance for future experiments and theoretical developments. Furthermore, this study enhances the Gibbs free energy theory pertaining to the liquid–gas interface. It underscores the substantial contribution of noble gases in this region to volumetric energy as temperature increases. Additionally, we employed Monte Carlo simulations to analyze the effective thermal neutron multiplication factor, denoted as k_{eff}. Our analysis reveals a linear correlation between graphite density and uniform density as a function of temperature. For the 1D Molten Salt Reactor Experiment (MSRE) system, we employed the Mole code to conduct heat and mass transfer calculations. These computations enable us to ascertain the distribution of fuel temperature based on coefficients and thermal properties. We also studied delayed neutron precursors during fuel cycling, taking into account the drift of cycling fuel through Mole–Griffin coupling. Our model represents k_{eff} and β_{eff} across various volume flow rates and salinity compositions. Finally, this study leveraged xenon-135 for continuous on-line monitoring of fuel salts to investigate the impact of steady-state xenon-135 on the MSRE and to better understand its distribution. These efforts build upon previous research related to removal processes.

1. INTRODUCTION

The U.S. Department of Energy's Office of Nuclear Energy's NEAMS program develops advanced modeling and simulation tools using the MOOSE framework to accelerate the deployment of advanced nuclear energy technologies. In the Molten Salt Reactor Technology field, the focus is on developing tools to model reactor multi-physics phenomena, such as radiochemical particle tracking. This includes modeling the behavior of noble gases, which are highly volatile during phase transitions between gas and liquid phases, supported across various multi-physics technology domains.

The purpose of this report is to evaluate the off-gas properties of highly volatile noble gases using Mole code for multiphysics calculations. This report provides evaluation and calculation details to reproduce the depleted particle generation and mass transfer coefficient process in a molten salt reactor using coupled Mole and Griffin codes.

This report is structured as follows:

- Section 2. Semi-Empirical Model for Henry's Law Constant of Noble Gases in Molten Salts
  This section presents a theoretical understanding of the solubility of noble gases and its application to engineering.
- Section 3. Coupled Neutronics and Species Transport Simulation of MSRE
  This section explains the reactor conditions, k_{eff}, according to the overall flow rate using the Mole and Griffin codes.
- Section 4. Parameters of Neutron Diffusion Equation for Temperature Effect of MSRE
  This section summarizes temperature-dependent parameters and Fuel salts enter the MSRE core at temperatures ranging between 400 and 900 K due to nuclear reactions in the core region. Our goal was to identify the temperature-dependent parameters of the neutron diffusion equation.

- Section 5. Heat and Mass Transfer Coefficients in the MSRE This section covers the use of mass transfer coefficient and heat transfer coefficient codes to examine the MSRE. Utilizing data based on physical and thermochemical properties such as temperature and density from the MSRE, the coefficients were calculated using correlation methods.
- Section 6. Noble Gas Transport in MSRE
  This section explores the influence of steady-state xenon-135 on the MSRE. Previous research has shown that continuous on-line fuel salts with xenon-135 provides initial insights into the overall distribution of this isotope.
- Section 7. Demonstration of Off-Gas System for Noble Gases in MSRE
  This section demonstrated that the concentration of xenon in the gas phase originates from the xenon liquid phase, particularly significant in scenarios involving vaporization where volatile fission products can be carried along.

2. SEMI–EMPIRICAL MODEL FOR HENRYS LAW CONSTANT OF NOBLE GASES IN MOLTEN SALTS

Henry's Law Constant describes the proportionality of dissolved gas to the partial pressure of free gas in liquid-gas equilibrium systems, extending its application to mass transport scenarios. The study focuses on determining the solubility of noble gases in molten salt by utilizing Henry's law constant. Mathematical modeling incorporates the van der Waals radius of noble gases and molten salt temperature. Gibbs Free Energy calculations encompass contributions from surface and volume energies, with enthalpy and entropy derived accordingly. A comparative analysis between conventional methods and the proposed model is conducted, leading to a unified theory predicting Henry's gas constant, entropy, and enthalpy for noble gases in molten salt solutions. The unified theory predicts the Henry gas constant, entropy, and enthalpy for noble gases in molten salt solutions, utilizing a functional form dependent on the van der Waals radius and temperature. The methodology employs a multiple regression approach to determine surface and volume energy parameters, which remain consistent across various noble gas and molten salt combinations. The model's accuracy and generality can be experimentally validated, offering insights into chemical properties derived from surface and volume energies. The Henry's law constants for helium, neon, argon, krypton, and xenon were determined in 2LiF–(64–36 mol%) and LiF–NaF–KF (46.5–11.5–42.0 mol%) solutions, leading to the publication of a journal paper in Scientific Reports, an open-access scientific journal published by Nature Portfolio. The title is "Semi-empirical model for Henry's law constant of noble gases in molten salts" (Sci Rep 14, 12847, 2024) [2].

3. COUPLED NEUTRONICS AND SPECIES TRANSPORT SIMULATION OF MSRE

This work focuses on the development of a coupling between two codes: Mole, a molten salt reactor species transport code, and Griffin, a reactor physics code. The study investigates the tracking of delayed neutron precursors within the MSRE (Molten Salt Reactor Experiment), specifically accounting for variations in fuel flow velocity across the primary loop. Griffin performs neutron transport calculations using 11 energy groups, while Mole conducts species advection calculations with 6 delayed neutron precursor groups. Together, Mole and Griffin predict the spatial distribution of neutron flux and precursors within the MSRE.

The Mole–Griffin coupling is utilized to compute parameters such as k_{eff} (effective multiplication factor)

and β_{eff} (effective delayed neutron fraction) under different volumetric flow rates in the reactor. By analyzing the effect of fuel cycling on delayed neutron precursors using Mole, the study achieves satisfactory results in modeling the distribution of delayed neutrons, comparing scenarios from no fuel flow in a critical state to fuel circulation under constant flow conditions.

The study highlights the dynamic behavior of the MSRE system, particularly the drift of delayed neutron precursors in circulating fuel. The Mole–Griffin coupling effectively solves coupled differential equations describing neutron flux and delayed neutron precursors. Validated through comparisons of β_{eff} against MSRE reference data, the 1D MSRE model, integrated with an 11-group neutron flux model, accurately simulates spatial distribution characteristics in channel fluid flow scenarios. The topic is published in "Coupled neutronics and species transport simulation of the Molten Salt Reactor Experiment," Nuclear Engineering and Design, 417, p.112824, [3].

4. PARAMETERS OF NEUTRON DIFFUSION EQUATION FOR TEMPERATURE EFFECT OF MSRE

4.1 INTRODUCTION

The Mole code is an important component of the Nuclear Energy Advanced Modeling and Simulation (NEAMS) program, which provides specialized modeling and simulation tools for the design and development of MSRs [4, 5]. This code effectively handles the time-dependent mass transport of radionuclides during multiphase transitions. Taking into account thermophysical properties, thermochemical properties, and phase equilibrium, Mole accurately predicts the fuel cycle and continuous loop formation of an MSR under transient or steady-state conditions. In this study, we investigated the reactor characteristics according to temperature change while performing macroscopic cross sections–based nuclear parameter analysis using the Serpent 2 Monte Carlo code [6]. The Mole code has also been enhanced to include the Bateman equations for nuclear transmutation and radioactivity involving fission fragments and neutron sources. In particular, the noble metal concentration, which exhibits a characteristic bubbling effect over an operating period of approximately 30 years, is a time-dependent equation that is solved and evaluated within the simulation.

Mole is a dedicated multiphysics application tailored to couple neutrons and temperature effects within MSRs. This study presents a comprehensive description of a 1D, one-group neutron model integrated with temperature effects. The model incorporates advection with delayed neutron precursor equations, allowing temperature-dependent calculations of 1D spatial distributions. This work verifies the reliability and accuracy of the methodology using Monte Carlo simulation results for the temperature-dependent parameters of the MSRE and is based on the data implemented for this purpose.

4.2 THEORY

The Mole code accurately simulates power reactor cores by integrating temperature-dependent macroscopic cross sections and critical state functions, which are derived from delayed neutron precursors. It incorporates fuel volume flow and flow-based fuel temperature feedback to ensure a comprehensive representation of core behavior. The following transient equations include a 1D, one-group neutron diffusion equation, 6-group delayed neutron precursor equations, and a heat transport equation. In each equation, The parameters needed for simulation and macroscopic cross-section data were obtained using Serpent2, a Monte Carlo reactor simulation code.. The equation can be solved for 1D, one-group neutron

diffusion with flowing delayed neutron precursors by spatial temperature distribution of the entire MSRE loop as

$$\frac{1}{v}\frac{\partial \phi}{\partial t} - \nabla \cdot (D\nabla\phi) + \Sigma_a \phi = (1-\beta)\,\nu\Sigma_f \phi + \sum_{i=1}^{I_N} \lambda_i C_i, \tag{1}$$

$$A\frac{\partial C_i}{\partial t} + \nabla \cdot (A\mathbf{u}C_i) = -A\lambda_i C_i + A\beta_i \nu\Sigma_f \phi, \quad i = 1, \ldots, 6 \tag{2}$$

$$A\rho_f c_p \frac{\partial T}{\partial t} + A\rho_f c_p \mathbf{u} \cdot \nabla T - \nabla \cdot \left(Ak_f \nabla T\right) = A\kappa\Sigma_f \phi. \tag{3}$$

In Eq. (1), v represents the neutron speed; and $\phi \equiv \phi\,(t, x)$ denotes the neutron flux with x ranging from 0 to H, where H corresponds to the height of the reactor. Additionally, $D \equiv (3\Sigma_{tr})^{-1}$ represents the diffusion coefficient, whereas Σ_a represents the macroscopic absorption cross section. Furthermore, Σ_f denotes the macroscopic fission cross section, and ν represents the average number of neutrons produced per fission reaction.

The parameter definitions of Eq. (2) are as follows: C_i represents the neutron concentration of precursor group i, whereas λ_i represents the decay constant of precursor group i. The symbol $\mathbf{u}$ represents the velocity of the molten salt, which is derived from the equation $Q = \mathbf{u}A$, where Q is the volume flow rate (operating at 1200 gpm in MSRE), and β_i corresponds to the fraction of delayed neutrons emitted per fission from precursor group i. Additionally, β represents the total fraction of delayed neutrons emitted from all precursor groups, given by the sum $\beta = \sum \beta_i$. A represents the cross-sectional area of the pipe and is not cancelable in both Eqs. 2 and 3 due to distinct values associated with each component of the MSRE, such as the heat exchanger and piping. Finally, the parameter definitions for Eq. (3) are as follows: the heat capacity of the liquid is denoted as c_p, the thermal conductivity is represented by k_f, the salt density is indicated by ρ_f, and κ represents the energy released per fission in MeV.

The temperature dependence of several parameters can be described as follows. The diffusion coefficient, denoted as D, can be expressed as a function of temperature: $D = D(T)$. The macroscopic cross section, represented by Σ_x, where $x \in \{a, f\}$, depends on temperature and can be calculated as the product of the atomic density $n_f(T)$ and the microscopic cross section $\sigma_x(T)$. The total delayed neutron ratio, denoted as β, also exhibits temperature dependence and can be described as $\beta = \beta(T)$. Furthermore, the delayed neutron ratio for a specific precursor group i, represented by β_i, is influenced by temperature and can be expressed as $\beta_i = \beta_i(T)$. Otherwise, temperature does not affect the values of λ_i, which represents the decay constant of precursor group i, κ (MeV/fission), and ν.

4.3 RESULTS AND ANALYSIS

The MSRE's fuel was UF_4 dissolved in a molten salt mixture. The primary loop, where the fuel enters the reactor vessel at a temperature of 908 K and exits at a temperature of 936 K as the molten salt, circulates to the pump. The reactor was designed for a power output up to 8 MWt, and the primary loop salt is LiF-BeF_2-ZrF_4-UF_4. The coolant salt used in the heat exchanger of the secondary loop comprises LiF-BeF_2. The molecular compositions for the fuel and coolant salt are shown in Table 1 along with the lithium and uranium atomic fractions. The MSRE utilizes fuel molten salt and graphite reflectors to promote salt flow and minimize hard neutron leakage in the core.

For 3D reactor physics calculations, the Serpent code, version 2.2.1, was employed. The reaction rates used in the calculations were obtained from the ENDF/B-VII.1 dataset. In Serpent2, cross sections are generated

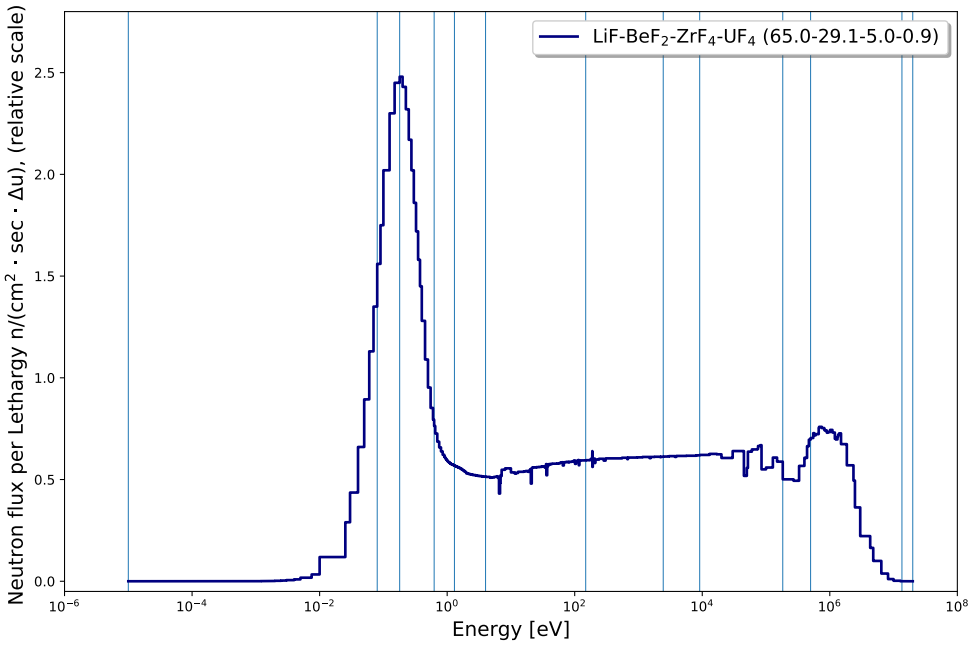

Figure 1. The normalized neutron flux distribution (per unit surface) is effectively homogenized for all materials in the MSRE and is presented based on the neutron energy distribution.

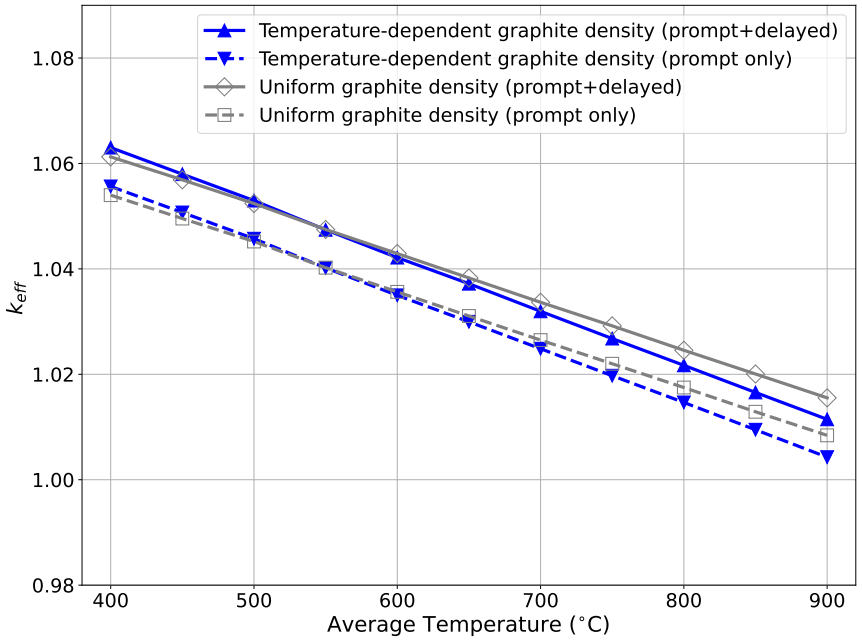

Figure 2. For the four cases, $k_{\mathbf{eff}}$ was determined to be temperature dependent and to have uniform graphite density for both (prompt+delayed) and (prompt only).

Table 1. Properties of the MSRE fuel salt. [1]

Property	Value	Units
MSRE fuel salt	LiF-BeF_2-ZrF_4-UF_4	(65.0-29.1-5.0-0.9) % mole.
Coolant salt	LiF-BeF_2	(66–34) % mole
Lithium composition	^{7}Li and ^{6}Li	99.9926% and 0.0074% mole
Uranium composition	^{234}U, ^{235}U, ^{236}U, ^{238}U	0.3-35-0.3-64.4 % mole
Liquidus temperature	433.89	°C
Surface tension	$\gamma(T) = 260 - 0.12T(^\circ\mathrm{C})$	erg/cm^2
Viscosity	$\mu_f(T) = 0.116 \exp[3755/T(^\circ\mathrm{K})]$	mPa−s
Salt density	$\rho_f(T) = 2.575 - 5.13 \times 10^{-4} T(^\circ\mathrm{C})$	g/cm^3
Temperature-dependent graphite density*	$\rho_g(T) = 1.891 - 3.35 \times 10^{-5} T(^\circ\mathrm{K})$	g/cm^3
Uniform graphite density	$\overline{\rho_g} = 1.86$	g/cm^3
Heat Capacity Liquid	$c_p = 0.47$	cal/g/°C
Thermal conductivity	$k_f = 0.0144$	W/cm/°C

* Graphite density linear model based on temperature over a range of densities

Table 2. Reactivity changes using linear regression, y=ax+b

	Linear regression	
Density	a	b
Functional graphite ρ_g, (p + d)	-9.96912×10^{-5}	0.101195
Functional graphite ρ_g, (p only)	-9.99072×10^{-5}	0.094391
Uniform graphite ρ_g, (p + d)	-8.84851×10^{-5}	0.095083
Uniform graphite ρ_g, (p only)	-8.87311×10^{-5}	0.088278

for transmutation and fission reactions for a one-group system representing average energies. The reaction rate of the average cell value is determined by calculating the neutron-induced reaction flux. Figure 1 of the normalized neutron flux (per unit lethargy) presents the distribution of neutron energy homogenizing all materials for the reactor. This neutron flux dominates thermal energy over fast thermal neutron energy in the MSRE. The effective multiplication factor k_{eff} is calculated for MSRE fuel salts composed of lithium and uranium components, as shown in Fig. 2. The four cases are determined by the disparity between (prompt + delayed) and (prompt only) while considering both temperature-dependent and uniform graphite densities.
These definitions are as follows:

- $k_{\mathrm{eff}}(\rho_g(T))$ is the temperature-dependent graphite density for prompt neutrons with delayed neutron precursors.
- $k_{\mathrm{p}}(\rho_g(T))$ is the temperature-dependent graphite density for prompt neutrons only.
- $k_{\mathrm{eff}}(\overline{\rho_g})$ is the uniform graphite density for prompt neutrons with delayed neutron precursors.
- $k_{\mathrm{p}}(\overline{\rho_g})$ is the uniform graphite density for prompt neutrons only.

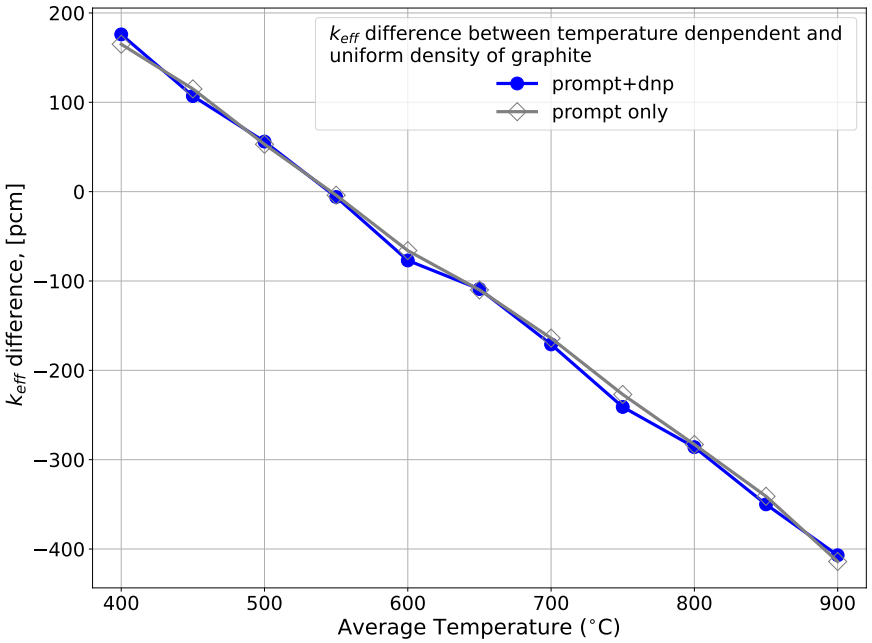

Figure 3. $k_{\mathbf{eff}}(\rho_g(T)) - k_{\mathbf{eff}}(\overline{\rho_g})$ **[blue line] and** $k_{\mathbf{p}}(\rho_g(T)) - k_{\mathbf{p}}(\overline{\rho_g})$ **[gray line].**

Figure 3 shows $k_{\text{eff}}(\rho_g(T)) - k_{\text{eff}}(\overline{\rho_g})$ and $k_{\text{p}}(\rho_g(T)) - k_{\text{p}}(\overline{\rho_g})$. On the other hand, Figure 4 shows $k_{\text{eff}}(\rho_g(T)) - k_{\text{p}}(\rho_g(T))$ and $k_{\text{eff}}(\overline{\rho_g}) - k_{\text{p}}(\overline{\rho_g})$. These comparisons of Figures 3 and 4 indicate that the difference decreases as the temperature increases. The results for the temperature dependence and uniform graphite densities in terms of k_{eff} show a significant difference in the effect of the temperature dependence on the graphite density.

The change in reactivity resulted from variations in both the average graphite density and the temperature dependency of the fuel salt. As shown in Figure 5, the slope of linear regression is known as the reactivity coefficient, a, due to change of temperature. Its value can be obtained as follows:

$$a = \frac{\mathrm{d}\ln(k_{\text{eff}})}{\mathrm{d}T} = \frac{1}{k_{\text{eff}}}\frac{\mathrm{d}k_{\text{eff}}}{\mathrm{d}T}. \tag{4}$$

The linear regression data are presented in Table 2. As for reactivity, the value of (prompt + delay) is lower than that of (prompt only). The delayed neutron fractions and decay constants for 6-group precursors are presented in Table 3. As the temperature increases, the delayed neutron fraction also rises. However, statistically, the uncertainty associated with these changes does not demonstrate a significant difference at a constant value with respect to temperature. The decay constant remains independent of temperature. The neutron speeds, which are dependent on temperature, are shown in Figure 6. Both the macroscopic cross sections of absorption and $\nu\Sigma_f$ are influenced by temperature and density variations (temperature-dependent and uniform) as shown in Figures 7 and 8, whereas the diffusion coefficients are solely dependent on temperature, as shown in Figure 9. κ (MeV/fission) has a constant value of 202.2765.

4.4 CONCLUSIONS

The k_{eff} analysis documented in this work utilized 3D Monte Carlo simulations with Serpent2 to investigate the temperature dependence of critical conditions. The obtained results reveal a linear correlation between

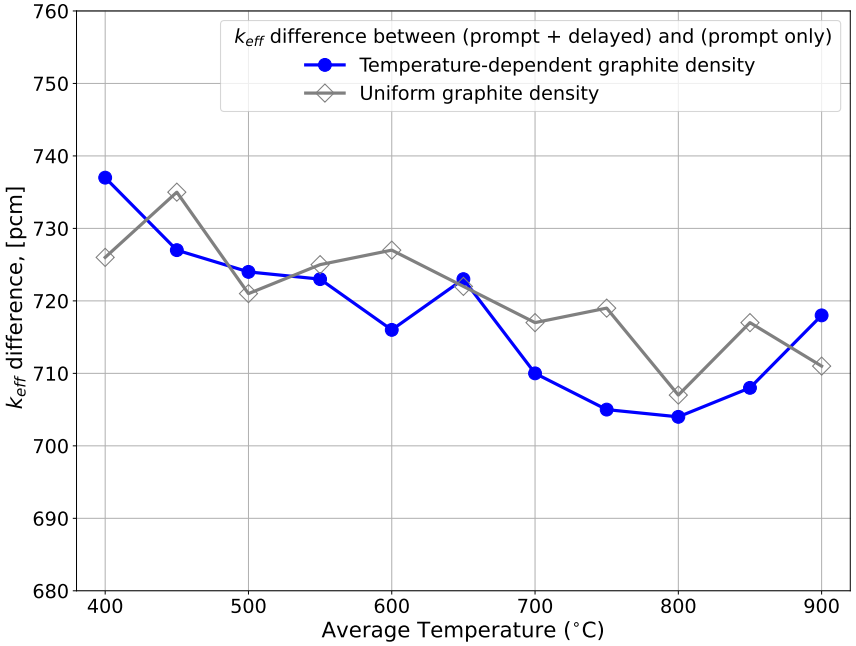

Figure 4. Difference in k_{eff} between prompt + delayed and prompt only neutrons cases for temperature-dependent and uniform graphite density.

the linear temperature-dependent graphite density and uniform graphite density.

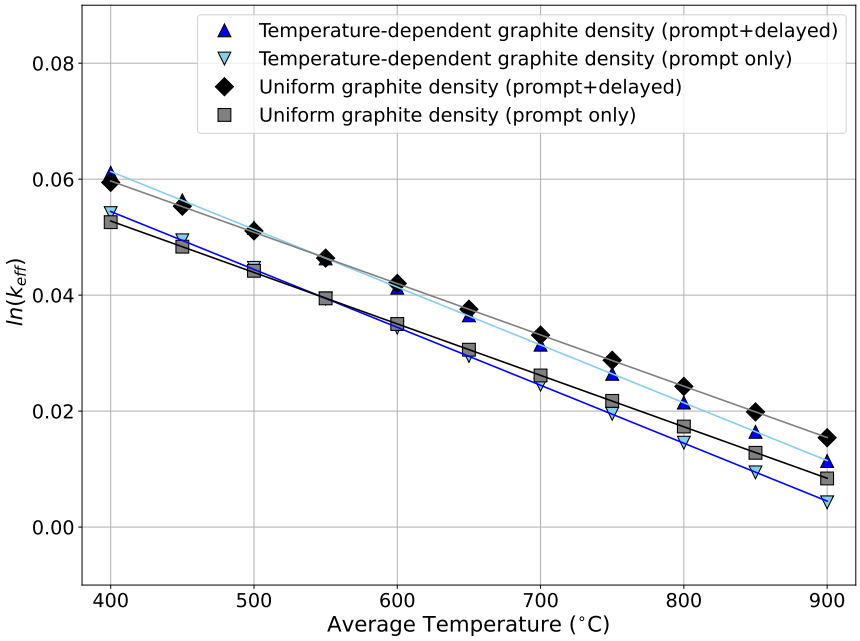

Figure 5. Reactivity coefficients calculated from linear regression.

Table 3. β_0, delayed neutron fractions and decay constants for 6-group precursors.

Fraction	Uniform	Functional
Total β_0	0.00641712	0.00636377
β_{01}	0.00022442	0.00022226
β_{02}	0.00115935	0.00114900
β_{03}	0.00110623	0.00109694
β_{04}	0.00248122	0.00246091
β_{05}	0.00101878	0.00101098
β_{06}	0.00042712	0.00042368
Decay Constant	sec^{-1}	
λ_1	0.01334	
λ_2	0.03274	
λ_3	0.12079	
λ_4	0.30284	
λ_5	0.84974	
λ_6	2.85377	

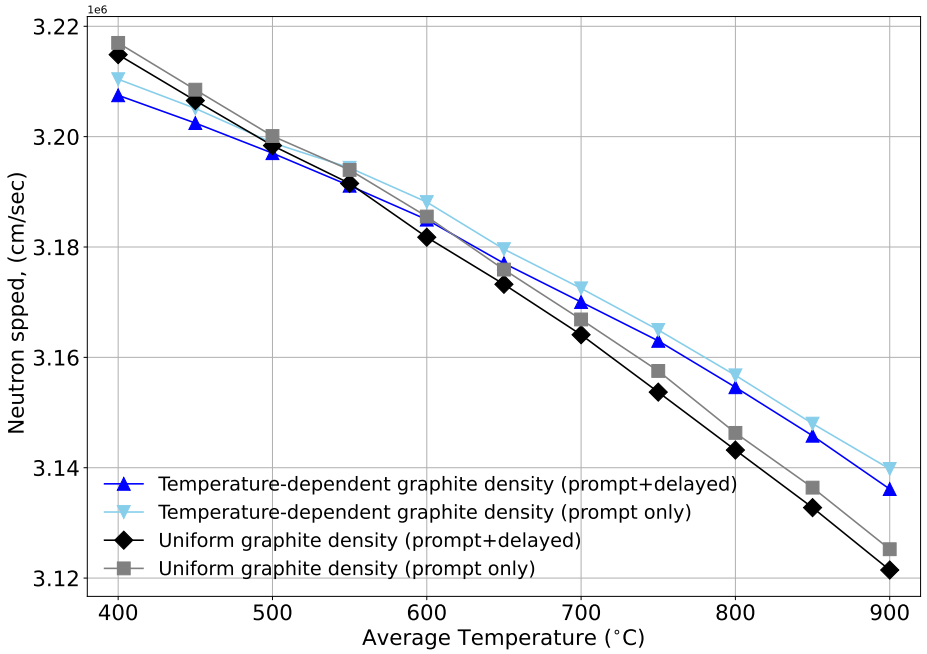

Figure 6. The neutron speed (cm/sec) shown as a function of temperature.

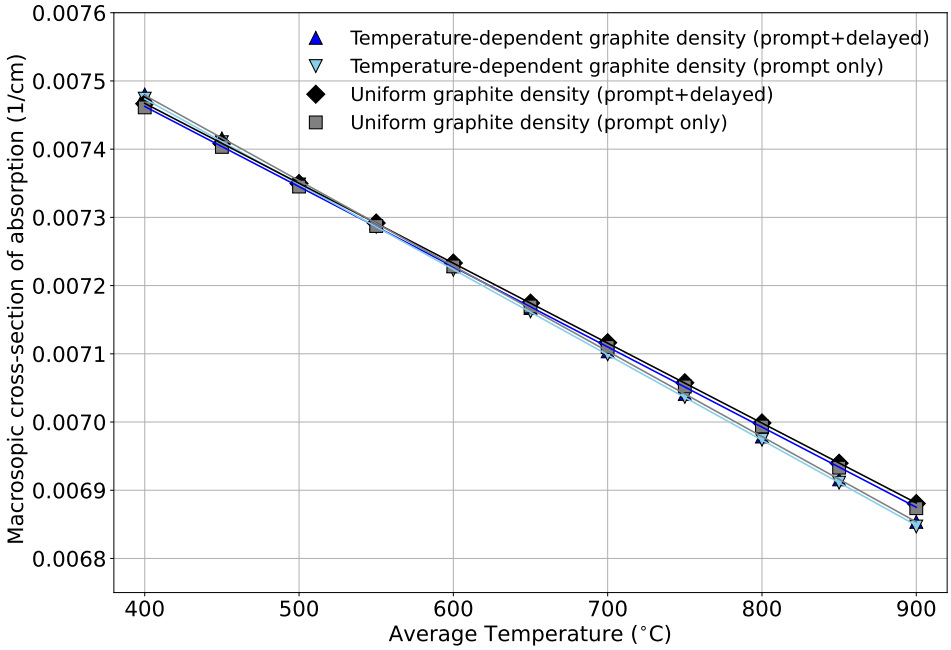

Figure 7. The macroscopic cross sections of absorption by average temperature.

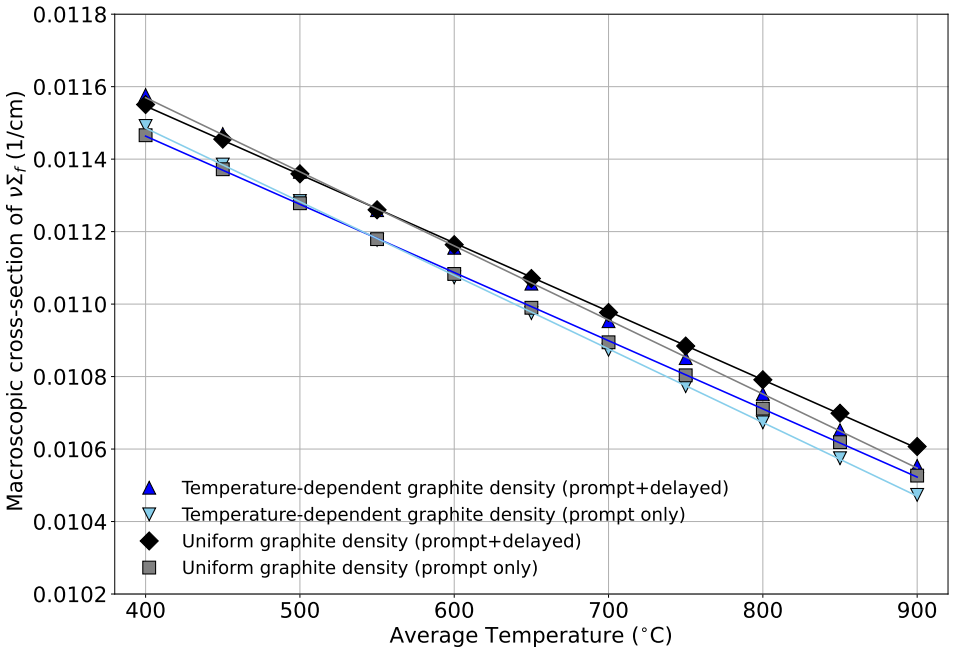

Figure 8. The macroscopic cross sections of $\nu\Sigma_f$ by average temperature).

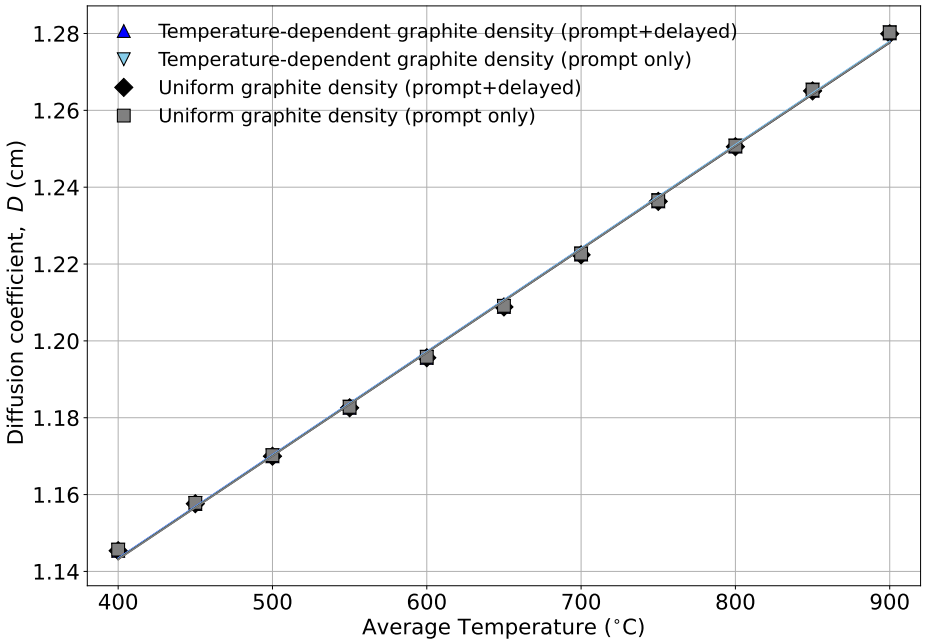

Figure 9. Diffusion coefficients by average temperature.

5. HEAT AND MASS TRANSFER COEFFICIENTS IN THE MSRE

5.1 INTRODUCTION

The Mole code, a dedicated multiphysics application specifically designed for MSRs, enables investigation of radiochemical species in the NEAMS program, which develops specialized tools for the modeling and simulation of MSRs. This code efficiently handles the time-dependent mass transport of radionuclides during various phase transitions. By considering thermophysical and thermochemical properties, as well as phase equilibrium, Mole accurately predicts the fuel cycle and continuous loop formation of chemical species for an MSR under both transient and steady-state conditions. In this study, mass transfer coefficient and heat transfer coefficient codes were employed to examine the MSRE. Utilizing data implemented based on physical and thermochemical properties such as temperature and density from the MSRE, the mass transfer coefficient and heat transfer coefficient were calculated using correlation methods.

5.2 THEORY

Mole is capable of handling time-dependent or steady-state mass transport and heat transfer, specifically for the transport of radionuclides during multiphase transitions [4, 5]. Furthermore, this code has been recently enhanced to incorporate the Bateman equations, enabling the simulation of nuclear transmutation and radioactivity involving fission fragments and neutron sources. The heat and mass transfer equations within Mole can be described by the following equations [7]:

$$J = k_w \left(c^* - c\right), \tag{5}$$

$$q = h \left(T^* - T\right), \tag{6}$$

where J is the flux of mass transfer, and q is the heat flux with boundary c^* and T^*, where superscript* indicates wall concentration or wall temperature, respectively. For the diffusion coefficient, two equations are commonly used for the liquid case: (1) the Stokes–Einstein equation and (2) the Wilke–Chang equations. The diffusivity in liquids can be calculated using the Stokes–Einstein equation:

$$D = \frac{k_B T}{6\pi \mu_f r_0} \left[\frac{\mathrm{cm}^2}{\mathrm{sec}}\right], \tag{7}$$

where k_B is the Boltzmann constant ($1.38064852 \times 10^{-16}$ in erg/K or $\mathrm{g} \cdot \mathrm{cm}^2/(\mathrm{s}^2 \cdot \mathrm{K})$), $\mu_f(T)$ is the dynamic viscosity in $\mathrm{g}/(\mathrm{cm} \cdot \mathrm{sec}) = 100\,\mathrm{cP}$, and r_0 is the solute radius in pm (1×10^{-10}cm). The diffusivity in liquids can also be determined using the Wilke–Chang equations [8]:

$$D = \frac{7.4 \times 10^{-8} (\phi M)^{0.5} T}{\mu_f V_B^{0.6}} \left[\frac{\mathrm{cm}^2}{\mathrm{sec}}\right] \tag{8}$$

where ϕ is the association factor of the solvent, M is the molecular weight of the solvent in g/mol, $\mu_f(T)$ is the dynamic viscosity in $\mathrm{mPa} \cdot \mathrm{sec}$, and V_B is the molar volume of the solute at its boiling point in $\mathrm{cm}^3/\mathrm{mol}$. The dimensionless numbers play a crucial role in analyzing fluid flow and heat and mass transfer

phenomena within the system. These numbers are calculated as follows:

$$\mathrm{Re} = \frac{\rho_f |\mathbf{u}| L}{\mu_f} \quad \text{Reynolds number} \tag{9}$$

$$\mathrm{Sc} = \frac{\mu_f}{\rho_f D} \quad \text{Schmidt numbers} \tag{10}$$

$$\mathrm{Sh} = \frac{k_w L}{D} \quad \text{Sherwood number} \tag{11}$$

$$\mathrm{Pr} = \frac{c_p \mu_f}{k_f} \quad \text{Prandtl number} \tag{12}$$

$$\mathrm{Nu} = \frac{hL}{k_f} \quad \text{Nusselt number} \tag{13}$$

In Eqs. (14–18), ρ_f represents the density of the fluid. μ_f is the dynamic viscosity of the fluid, which describes its resistance to flow. $\mathbf{u}$ signifies the velocity of the fluid. The characteristic length of the system, such as the pipe diameter, is denoted by L. The diffusion coefficient, represented by D, characterizes the rate at which mass is transported through the fluid. k_w is the mass transfer coefficient specifically related to wall deposition, describing the effectiveness of mass transfer between the fluid and the wall. The thermal conductivity of the fluid is denoted by k_f, indicating its ability to conduct heat. c_p represents the specific heat of the fluid, which measures the amount of heat required to raise its temperature by a certain amount. h represents the convective heat transfer coefficient, which determines the heat transfer rate between the fluid and its surroundings through convection.

Table 4. Properties of the MSRE fuel salt. [1]

Property	Value	Units
MSRE fuel salt	LiF-BeF_2-ZrF_4-UF_4	(65.0-29.1-5.0-0.9) % mole.
Coolant salt	LiF-BeF_2	(66–34) % mole
Lithium composition	^{7}Li and ^{6}Li	99.9926% and 0.0074% mole
Uranium composition	^{234}U, ^{235}U, ^{236}U, ^{238}U	0.3-35-0.3-64.4 % mole
Liquidus temperature	433.89	°C
Surface tension	$\gamma(T) = 260 - 0.12T(^\circ\mathrm{C})$	erg/cm^2
Viscosity	$\mu_f(T) = 0.116 \exp[3755/T(^\circ\mathrm{K})]$	mPa−s
Salt density	$\rho_f(T) = 2.575 - 5.13 \times 10^{-4} T(^\circ\mathrm{C})$	g/cm^3
Heat Capacity Liquid	$c_p = 0.47$	cal/g/°C
Thermal conductivity	$k_f = 0.0144$	W/cm/°C

The Dittus–Boelter equation in circular tubes is

$$\mathrm{Sh} = 0.023\mathrm{Re}^{0.8}\mathrm{Sc}^n \quad \mathrm{Nu} = 0.023\mathrm{Re}^{0.8}\mathrm{Pr}^n, \tag{14}$$

where $n = 0.4$ for heating, and $n = 0.3$ for cooling. The heat and mass transfer coefficients, denoted as h and k_w, respectively, are determined by the relationship derived from the Dittus–Boelter equation.

$$k_w = 0.023\frac{D}{L}\mathrm{Re}^{0.8}\mathrm{Sc}^n \quad \text{and } h = 0.023\frac{k_f}{L}\mathrm{Re}^{0.8}\mathrm{Pr}^n \tag{15}$$

Table 5. Fuel fluid parameters in fuel circulating loop of MSRE at 1200 gpm.

	Volume [9]		Residence	Mean velocity		Length	Cross-sectional
	ft^3	cm^3	Time, τ (sec)	u (cm/sec)	(ft/sec)	L (cm)	area, A_{eff} (cm^2)†
Pump $^{10\to1}$	1.10	3.1149×10^4	0.41	585.22	19.20	240.77	1.294×10^2
Fuel Loop Piping $^{1\to2}$	0.76	2.1521×10^4	0.28	585.22	19.20	166.35	1.294×10^2
Heat Exchanger $^{2\to3}$	6.12	1.7330×10^5	2.29	106.53	3.50	243.84	7.107×10^2
Fuel Loop Piping $^{3\to4}$	2.18	6.1731×10^4	0.82	585.22	19.20	477.17	1.294×10^2
Outer annulus $^{4\to5}$	9.72	2.7524×10^5	3.64	167.64	5.50	609.46	4.516×10^2
Lower plenums $^{5\to6}$	12.24	3.4660×10^5	4.58	6.66	0.22	30.50	1.136×10^4
Reactor vessel core $^{6\to7}$	23.52	6.6601×10^5	8.80	21.34	0.70	187.69	3.548×10^3
Upper plena $^{7\to8}$	11.39	3.2253×10^5	4.26	6.65	0.22	28.38	1.136×10^4
Fuel Loop Piping $^{8\to9}$	1.37	3.8794×10^4	0.51	585.22	19.20	299.87	1.294×10^2
Fuel Loop Piping $^{9\to10}$	0.73	2.0671×10^4	0.27	585.22	19.20	159.79	1.294×10^2
Total	69.13	1.9575×10^6	25.86	—	—	—	—

† Volumetric flow rate, 1200 gpm is $Q = A_{\text{eff}}\mathbf{u}$, where A_{eff} is the effective cross section and $\mathbf{u}$ is fluid velocity.

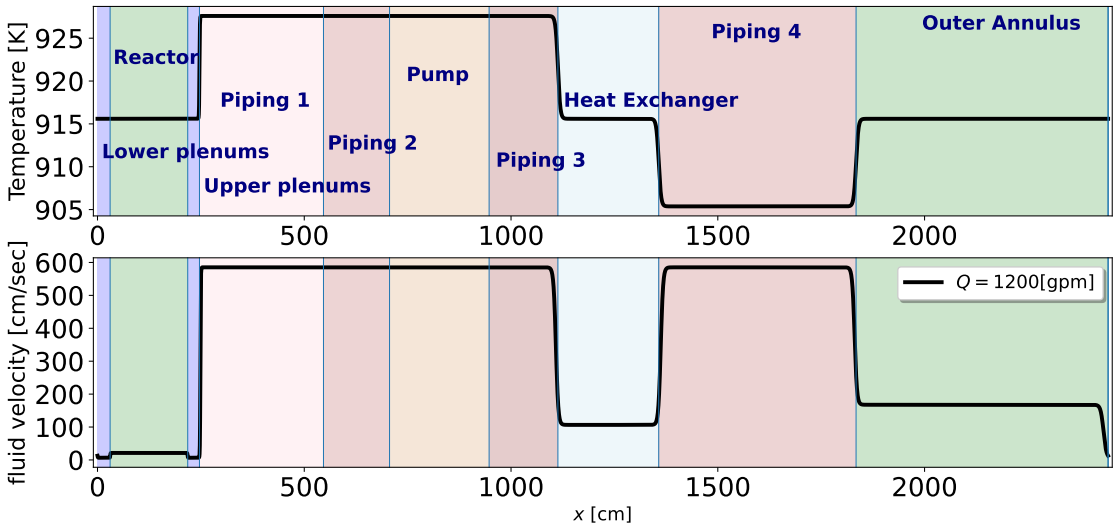

Figure 10. Temperature (top) and fluid velocity (bottom) distribution of MSRE loop.

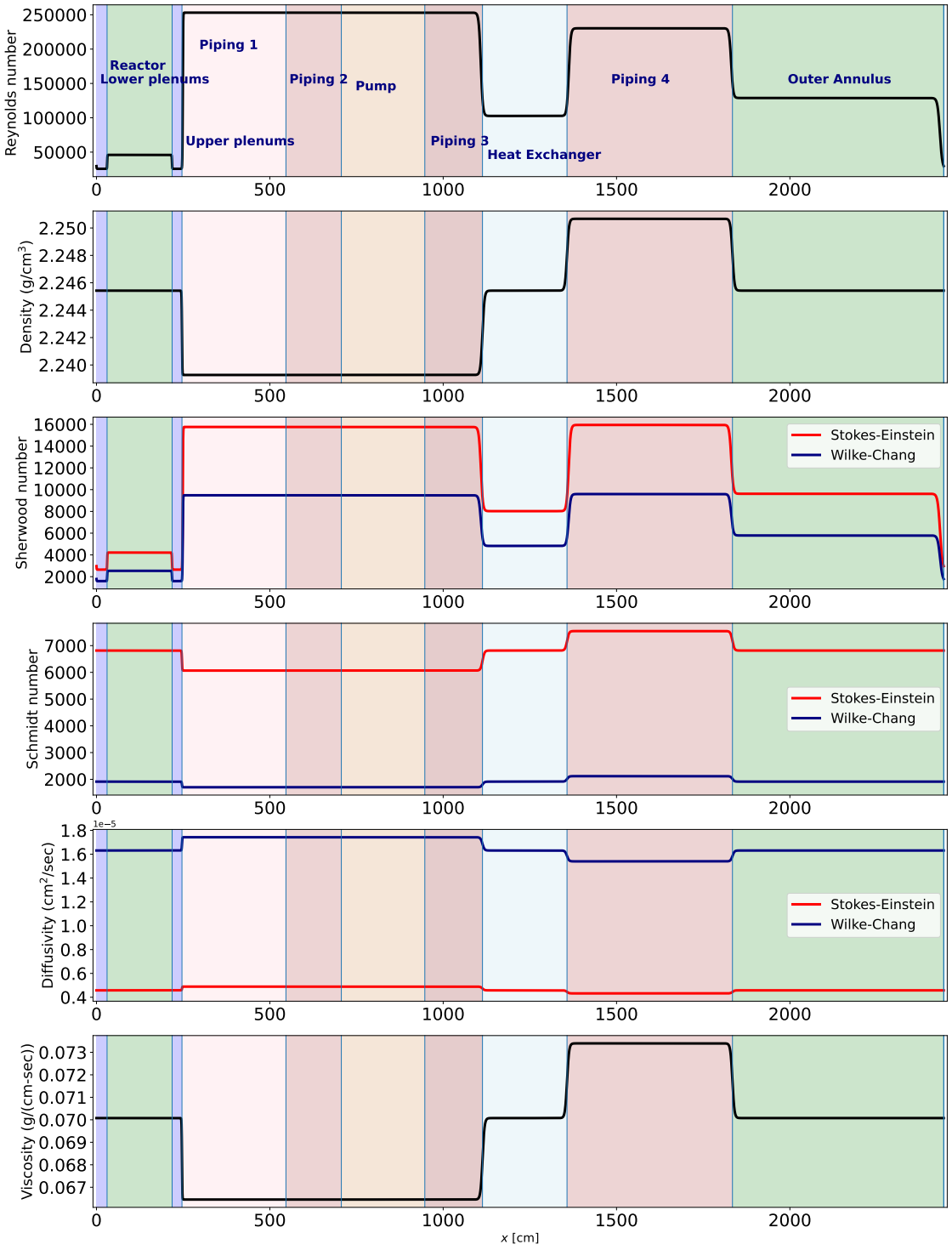

Figure 11. Properties of density and Sherwood, Schmidt, and Reynolds numbers and diffusivity of the MSRE Fuel Salt.

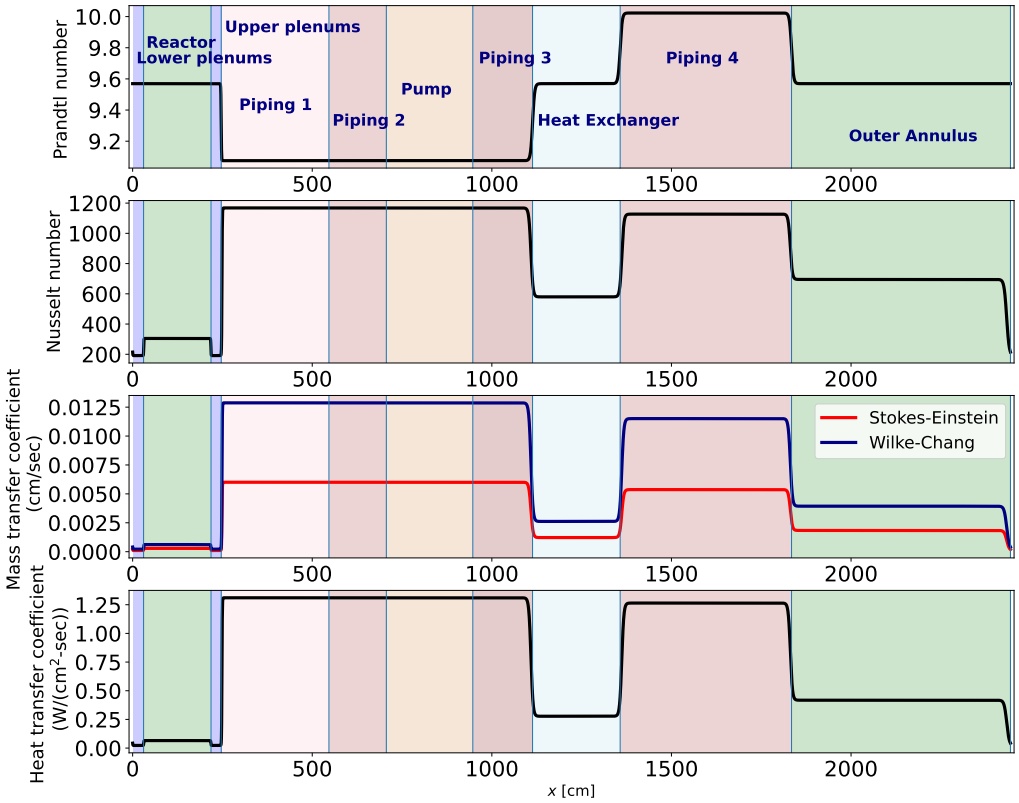

Figure 12. Properties of mass transfer coefficients with Stokes–Einstein and Wilke–Chang methods, heat transfer coefficient, Prandtl number, and Nusselt number.

5.3 RESULTS AND ANALYSIS

The fluid properties module of MOOSE utilizes the properties of saline. In Figures 10, 11, and 12, dimensionless parameters—such as diffusion coefficients for heat and mass transfer—are presented using Tables 4 and 5. The colors in Figures 10, 11, and 12 align with each component in Table 5, with lower plena (5) on the left and outer annulus (4) on the right.

5.4 CONCLUSIONS

To accurately simulate the spatial distribution shape for a 1D MSRE system, heat and mass transfer calculations were performed using the Mole code. The mass transfer coefficient is incorporated into the radioactive species trace, and the fuel temperature distribution is determined based on the heat transfer coefficient, heat capacity, and thermal conductivity.

6. NOBLE GAS TRANSPORT IN MSRE

6.1 INTRODUCTION

The development of the Mole code, designed for the analysis of MSRs, is a significant undertaking within the NEAMS program, which receives support from the US Department of Energy's Nuclear Energy Office. Mole operates seamlessly within the MOOSE framework, facilitating the integration of multiphysics simulations with other MOOSE-based applications. Its primary mission is to perform mass transfer transport simulations of radioactive chemical species, enabling predictions of nuclear and chemical reactions specific to MSRs. Mole's capabilities extend to addressing intricate scenarios, such as the movement of radioactive isotopes undergoing multiphase transitions. This encompasses phenomena like neutron activation, the migration of isotopes from system components into the fluid, phase transitions, gas-liquid species diffusion, and the deposition of species from the fluid onto system components. Importantly, the Mole architecture is designed to seamlessly interface with other physics codes, enabling it to track and update the spatial distribution of species and share this updated distribution with other codes. This feature is crucial for addressing safety and licensing concerns unique to MSRs, often necessitating multiphysics simulations.

Within the MOOSE framework, a key integration exists with the Griffin neutron transport code, which shares a close relationship with Mole [4, 5, 10]. Griffin provides fission source distributions to Mole, and Mole reciprocates by supplying updated isotope distributions back to Griffin. This coupling ensures efficient simulations, accommodating both SingleApp and MultiApp systems, thus enabling parallel execution at distinct mesh levels. These simulations can operate in steady-state or transient modes, offering the flexibility to employ varying time steps for transient calculations in each code. This tight integration empowers Mole to contribute to the computation of reactor neutron flux distributions, considering the transport and decay of fission products beyond the active core region. Although the primary focus of this work centered on delayed neutron precursors, the analysis presented here can readily extend to address other facets of MSRs. These computational strategies and data are of paramount importance within the NEAMS domain, particularly in the context of macroscopic engineering-scale multiphysics simulations for MSRs. The synergy between Mole and Griffin is poised to enhance the diverse capabilities of NEAMS.

6.2 METHOD

The governing equation that describes neutron diffusion within an MSR, as derived from Griffin, takes the form of a multigroup neutron diffusion equation:

$$\frac{1}{v_g}\frac{\partial \phi_g}{\partial t} - \nabla \cdot \left(D_g \nabla \phi_g\right) + \Sigma_{t,g}\phi_g = \sum_{g'=1}^{G} \Sigma_{s,g'\to g}\phi_{g'} + \left(1 - \sum_{i=1}^{N}\beta_i\right)\sum_{g'=1}^{G}\chi_{p,g'\to g}\nu_{g'}\Sigma_{f,g'}\phi_{g'} + \sum_{i=1}^{N}\chi_{d,i,g}\lambda_i C_i, \quad g \in [1,\ldots,G]. \tag{16}$$

In this equation, the various parameters and terms are defined as follows:

v_g is the neutron speed for group g.
D_g is the diffusion coefficient for group g.

$\Sigma_{t,g}$ is the total macroscopic cross section for group g.
ν_g is the average number of neutrons produced per fission reaction for group g.
$\Sigma_{f,g}$ is the fission macroscopic cross section for group g.
$\Sigma_{s,g'\to g}$ is the macroscopic scattering cross section from group g' to g.
β_i is the fraction of fission delayed neutrons for precursor group i.
$\chi_{p,g'\to g}$ is the energy distribution for prompt neutron fission from group g' to g.
$\chi_{d,i,g}$ is the energy distribution of the delayed neutron group for precursor group i.
λ_i is the decay constant of precursor group i.

In addition to neutron transport, the Mole code also deal with DNPs. DNPs in Mole are represented as 6-group fission fragments capable of emitting neutrons. These DNPs move at the same velocity as the liquid fuel. The neturon flux presents Griffin's solution of this governing equation to compute the group scalar fluxes from Eq. 16. The equation governing DNPs in a 1D closed-loop fuel flow system is expressed as follows:

$$A\frac{\partial C_i}{\partial t} + \frac{\partial}{\partial x}\left(Au_x^l C_i\right) = -A\lambda_i C_i + A\beta_i \sum_{g'=1}^{G} \nu_{g'}\Sigma_{f,g'}\phi_{g'}, \quad i \in [1,\ldots,N]. \tag{17}$$

Here, u_x represents the average fuel flow velocity in the x-direction, and A signifies the cross-sectional area of the flow path. Importantly, this equation takes into account periodic boundary conditions, ensuring continuity of circulation within the closed-loop fuel system.

For noble gas transport within Mole, the governing equations are utilized, one for the precursor (c_p^l), another for the liquid phase (c_j^l), and the third for the gas phase (p_j^g):

$$A\frac{\partial c_p^l}{\partial t} + \frac{\partial}{\partial x}\left(Au_x^l c_p^l\right) = A\gamma_p^c\Sigma_f\phi - A\lambda_p c_p^l - Ak_p^w a^w(c_p^l - c_p^s) + Ak_p^b a^b(c_p^l - c_p^b) + Ak_{re}a^{re}(c_p^\dagger - c_p^l), \tag{18}$$

$$\begin{aligned} A\frac{\partial c_j^l}{\partial t} + \frac{\partial}{\partial x}\left(Au_x^l c_j^l\right) &= A\gamma_j^c\Sigma_f\phi + A\lambda_p c_p^l - A\lambda_j c_j^l - Ak_l^w a^w(c_j^l - c_j^s) + Ak_l^b a^b(c_j^l - c_j^b) \\ &\quad + AK_L a^t(c_j^* - c_j^l), \end{aligned} \tag{19}$$

$$A\frac{\partial p_j^g}{\partial t} + \frac{\partial}{\partial x}\left(Au_x^g p_j^g\right) = A\gamma_j^p\Sigma_f\phi - A\lambda_j p_j^g - Ak_g^w a^w(p_j^g - p_j^s) + AK_G a^t(p_j^g - p_j^*) - A\xi\, p_j^g. \tag{20}$$

where
A is the cross-sectional area of each component.
c_p^s is the precursor concentration on the surface wall,
c_j^s is the liquid concentration on the surface wall,
c_j^b is the liquid concentration in the bubble,
c_j^* is the liquid–vapor interface concentration at transitions,
$c_p^\dagger$ is the precursor concentration at an oxidation-reduction reactions,
p_j^s is the vapor pressure on the surface wall,
p_j^b is the vapor pressure in the bubble,
p_j^* is the vapor–liquid interface pressure at transitions,

k_p^w is the precursor mass transfer coefficient into the wall,
k_l^w is the liquid mass transfer coefficient into the wall,
k_g^w is the vapor mass transfer coefficient into the wall,
k_p^b is the precursor mass transfer coefficient into the bubbles,
k_l^b is the liquid mass transfer coefficient into the bubbles,
k_{re} is the mass transfer coefficient of the oxidation-reduction reaction,
K_L is the overall liquid phase mass transfer coefficient for the liquid-into-vapor transition,
K_G is the overall vapor–liquid mass transfer coefficient for the liquid-into-vapor transition,
a^{re} is the interfacial area per unit volume of the oxidation-reduction reaction,
a^w is the interfacial area per unit volume on the wall,
a^b is the interfacial area per unit volume of liquid into the bubble,
a^t is the interfacial area per unit volume on the liquid-vapor transition,
λ_p is the precursor decay constant,
λ_j is noble gas decay constant,
u_x^l is salt fluid velocity,
u_x^g is vapor velocity,
γ_p^c is the yield rate of the precursor for the concentration unit
γ_j^c is the yield rate of noble gas for the concentration unit
γ_j^p is the yield rate of noble gas for the pressure unit, and
ξ the off-gas removal rate at pump.

These equations account for parameters and variables related to noble gas concentrations and pressures in both phases. The mass transfer coefficients, diffusion coefficients, and various constants involved are either determined from the technical literature or calculated using appropriate methods.

For instance, the mass transfer coefficients in the gas phase (K_G) and the liquid phase (K_L) are expressed as:

$$\frac{1}{K_G} = \frac{1}{k_l H} + \frac{1}{k_g} \qquad\qquad \frac{1}{K_L} = \frac{1}{k_l} + \frac{H}{k_g}, \tag{21}$$

Here, k_l represents the liquid phase mass transfer coefficient, k_g is the gas phase mass transfer coefficient, and H is Henry's law constant, which is the ratio of the concentration in the liquid phase to the pressure in the gas phase, The relationship is given by $c = pH$, where c is the liquid concentration and p is the pressure.

To calculate species diffusion coefficients (D) in liquid salt, the Wilke–Chang equation is employed:

$$D = \frac{7.4 \times 10^{-8} (\phi M)^{0.5} T(\mathrm{K})}{\mu_f V_B^{0.6}} \left[\frac{\mathrm{m}^2}{\mathrm{s}}\right], \tag{22}$$

where various parameters such as molecular weight of the solvent (M), molar volume at the boiling point (V_B), temperature in Kelvin (T), and viscosity of the liquid salt (μ_f) are incorporated into the calculation.

In the liquid phase, the mass transfer coefficient k_l is determined using the Dittus–Boelter equation for turbulent flow (Reynolds number, Re > 10,000) in circular tubes.

Overall, these equations and parameters constitute the foundation for understanding the complex multiphysics phenomena within MSRs. This encompasses neutron transport, delayed neutron precursors, and noble gas transport, among other critical processes. The interplay between these factors is essential for comprehending and optimizing MSR performance so as toaccount for numerous physical and chemical interactions.

The Reynolds number (Re) and Schmidt number (Sc) are fundamental parameters defined as follows:

$$\mathrm{Re} = \frac{\rho_f Q L}{\mu_f A} \qquad \text{Reynolds number} \tag{23}$$

$$\mathrm{Sc} = \frac{\mu_f}{\rho_f D} \qquad \text{Schmidt number} \tag{24}$$

To predict species diffusion coefficients, D, in liquid salt, we can apply the Wilke–Chang equation [8]:

$$D = \frac{7.4 \times 10^{-8} (\phi M)^{0.5} T(\mathrm{K})}{\mu_f V_B^{0.6}} \left[\frac{\mathrm{m}^2}{\mathrm{s}}\right]. \tag{25}$$

In this equation, M represents the molecular weight of the solvent, V_B is the molar volume at the boiling point, and ϕ is the solute factor (usually assumed as $\phi = 1$ for the salt case). T denotes the absolute temperature in Kelvin (K).

The relative velocity between the vapor and liquid phases in turbulent pipe flow is given by [11]:

$$u_r = u_x^g - u_x^l \tag{26}$$

Turbulent fluctuation is defined as $u' = u - \overline{u}$. The average and variance of the fluctuation velocity are expressed as

$$\overline{u_x^{g'}} = \overline{u_x^{l'}} = \frac{1}{T}\int_0^T (u - \overline{u}) dt = 0, \tag{27}$$

$$\overline{(u_x^{g'})^2} = \overline{(u_x^{l'})^2} = \frac{1}{T}\int_0^T (u - \overline{u})^2 dt \geq 0. \tag{28}$$

Therefore, the root mean square (RMS) values of vapor fluctuating velocity are equal to those of liquid fluctuating velocity:

$$\sqrt{\overline{(u_x^{g'})^2}} = \sqrt{\overline{(u_x^{l'})^2}}. \tag{29}$$

It is known that the acceleration of vapor is three times that of liquid flow [12]. The RMS velocity over a period of time can be equated to acceleration. Consequently, the relative velocity can be expressed as

$$u_r = u_x^g - u_x^l = 3\sqrt{\overline{(u_x^{g'})^2}} - \sqrt{\overline{(u_x^{l'})^2}} = 2\sqrt{\overline{(u_x^{l'})^2}}. \tag{30}$$

Additionally,

$$\sqrt{\overline{(u_x^{l'})^2}} \approx u_x^l \sqrt{\frac{f}{2}}. \tag{31}$$

The turbulence intensity is calculated by dividing the mean square fluctuation components by the mean absolute velocity. The friction factor relation is $f = 0.046\mathrm{Re}^{-0.2}$ for turbulent flow in a smooth tube, where $\mathrm{Re} = \rho_f u_x^l L/\mu_f$ [13].

In the context of MSRs, a technology designed for extracting nuclear fission product gas from fuel salt and efficiently removing noble gas using helium bubbles in the circulating fuel pump, there are significant theoretical challenges associated with interfacial area and mass transfer coefficient estimation. These factors play pivotal roles in representing mass transfer processes. The mass transfer coefficient from the fuel salt to the circulating bubbles is expressed as [14]:

$$k^b = 0.089\frac{D}{L}\mathrm{Re}^{0.69}\mathrm{Sc}^{0.33}. \tag{32}$$

The interfacial area of the wall exposed to the fuel salt can be calculated using the following equation:

$$a^w = \frac{s^w}{\mathrm{V}_i}, \tag{33}$$

where s^w represents the wall surface area of each component, and V_i denotes the volume of each component within the MSRE.

The gas phase holdup, a parameter closely related to interfacial area and the velocity of gas bubbles within a liquid medium, is defined as the ratio of the gas phase volume to the total volume. This parameter is established by Peebles in 1968 [11] and by Hightower in 1975 [15] for both the bubbly regime and the slugging regime:

$$\alpha = 0.322\left(\frac{\rho_l\left(u_x^g\right)^4}{g\sigma}\right)^{0.219} \quad \text{(Bubbly regime)}, \tag{34}$$

$$= 0.848\left(\frac{\left(u_x^g\right)^2}{gD_l}\right)^{0.362} \quad \text{(Slugging regime)}. \tag{35}$$

For circulating bubbles, the interfacial area a^b within bubble entrainment is determined by the gas phase holdup (bubble volume fraction) α and the Sauter mean diameter d_{32} of the circulating bubbles:

$$a^b = \frac{s^b}{\mathrm{V}i} = \frac{6\alpha}{d_{32}(1-\alpha)}, \tag{36}$$

where s^b is the total surface area of circulating bubbles, Vi is the volume of the salt liquid phase of each component, and d_{32} represents the Sauter mean diameter.

Similarly, the interfacial area of the liquid–vapor transition for noble gas is determined by:

$$a^t = \frac{s^t}{\mathrm{V}i} = \frac{6\alpha_j}{d_{32}^j(1-\alpha_j)}, \tag{37}$$

where s^t is the total surface area of liquid–gas transition, d_{32}^j is the Sauter mean diameter of noble gas vapors, α_j is the noble gas volume fraction of element j, and s^t is the total surface area of the noble gas vapors interface.

6.3 RESULTS

$$\boxed{{}^{135}_{53}\mathrm{I}} \xrightarrow[6.57(2)\ \mathrm{hr}]{\beta^-} \boxed{{}^{135}_{54}\mathrm{Xe}} \xrightarrow[9.14(2)\ \mathrm{hr}]{\beta^-} \boxed{{}^{135}_{55}\mathrm{Cs}}$$

Figure 13. Simple decay chain of $^{135}_{54}$Xe.

Preliminary assessments of neutron flux and delayed neutron precursor values were conducted for the purpose of validating noble gas calculations against the MSRE as shown in the Figures 14 and 15. Xenon-135 exerts a significant negative impact on reactor operation due to its strong neutron-absorbing properties. This radioactive isotope is generated through the decay of the fission product iodine-135, which subsequently transforms into cesium-135, as shown in Figure 13. Xenon-135 has liquid and gas phases. The liquid phase means that xenon gas is dissolved in molten salts, whereas in the gas phase xenon presents bubble behaviors. The results are presented in Figures 16, 17, and 18. At steady state, the primary loop of the MSRE contains distributions of iodine and xenon concentrations.

6.4 CONCLUSION

The present study explores the influence of steady-state xenon-135 on the MSRE. Previous research conducted with MSRE has demonstrated that continuous on-line inert gas stripping of fuel salts with xenon-135 can yield initial insights into the overall distribution of this isotope.

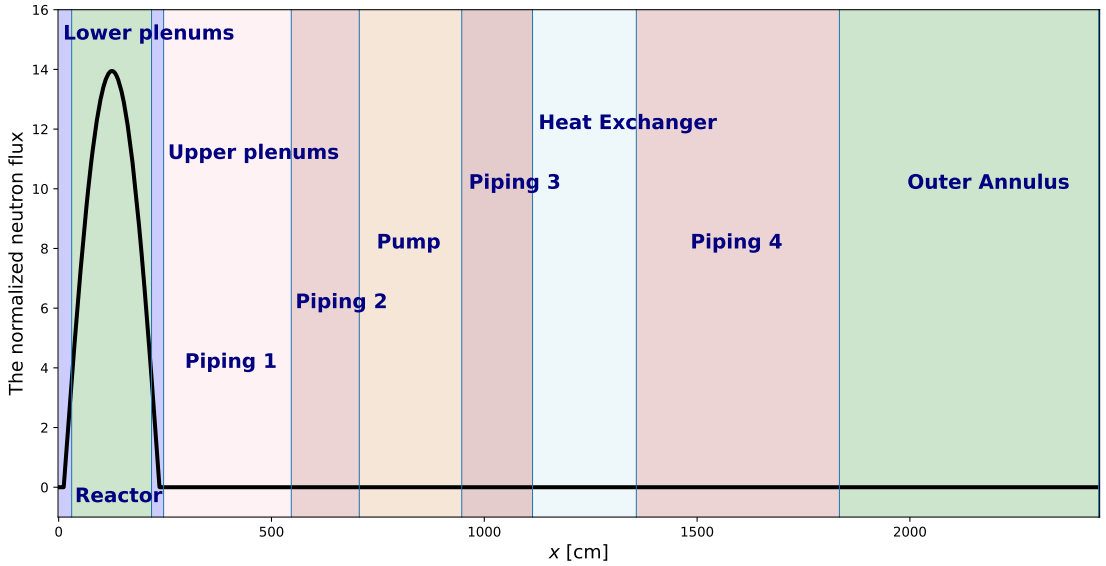

Figure 14. The normalized neutron flux distribution of MSRE 1D loop.

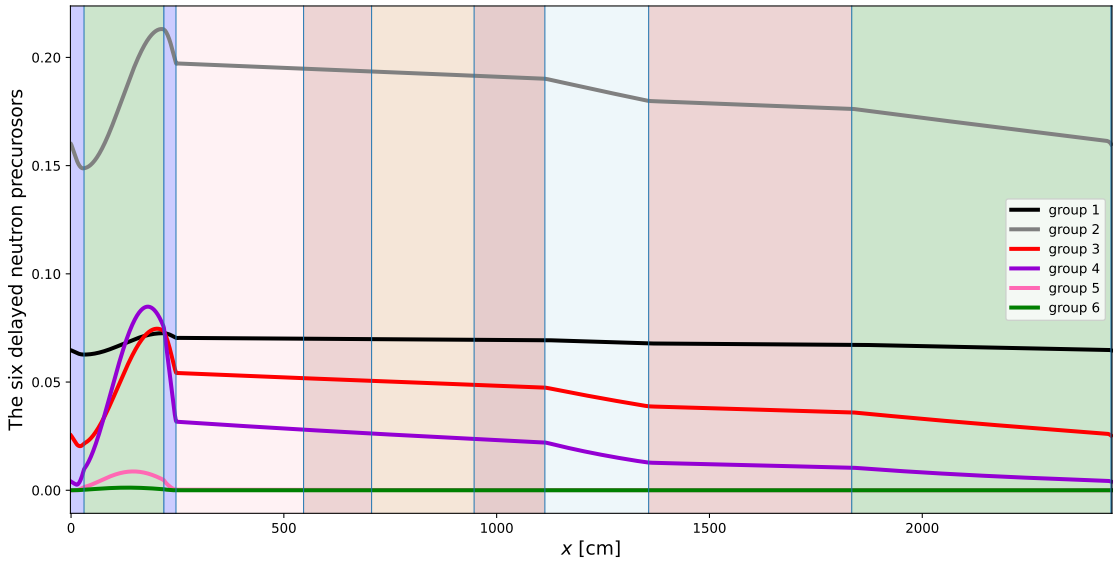

Figure 15. The 6 groups delayed neutron precursors of MSRE 1D loop.

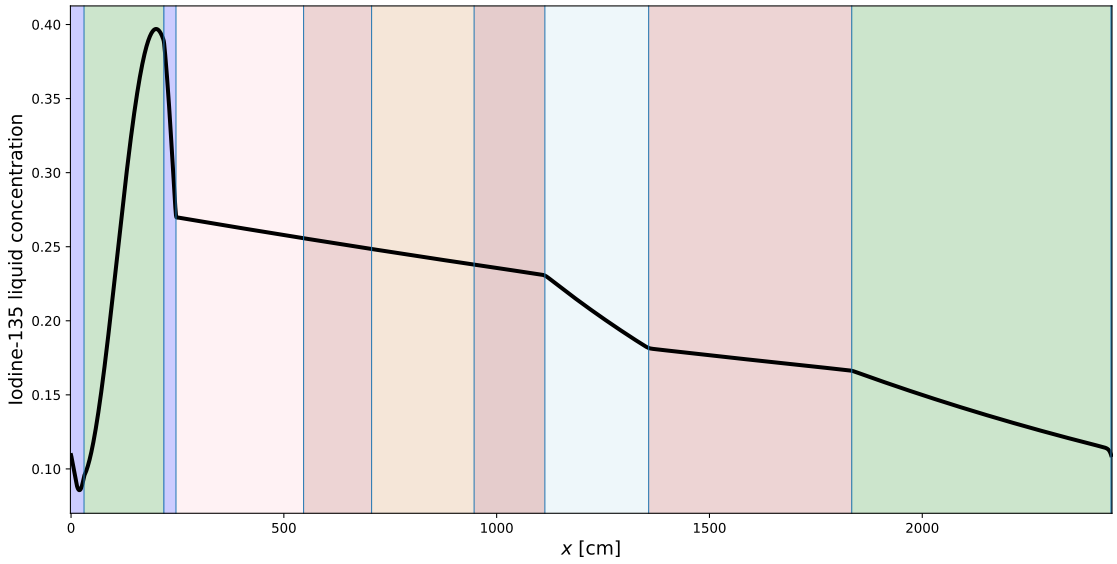

Figure 16. Iodine liquid concentration distribution of MSRE 1D loop.

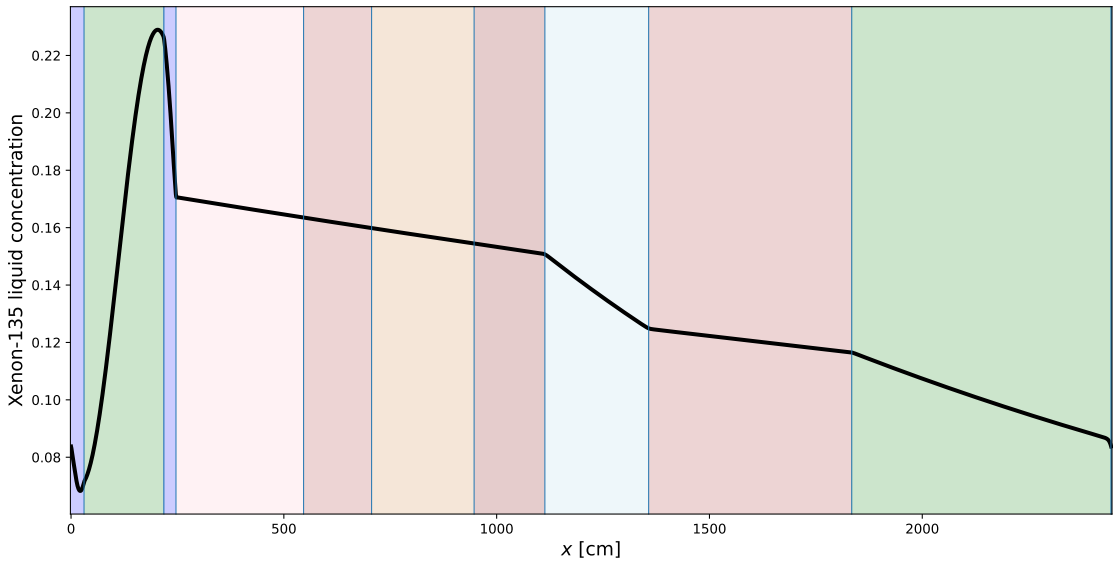

Figure 17. Xenon liquid concentration distribution of MSRE 1D loop.

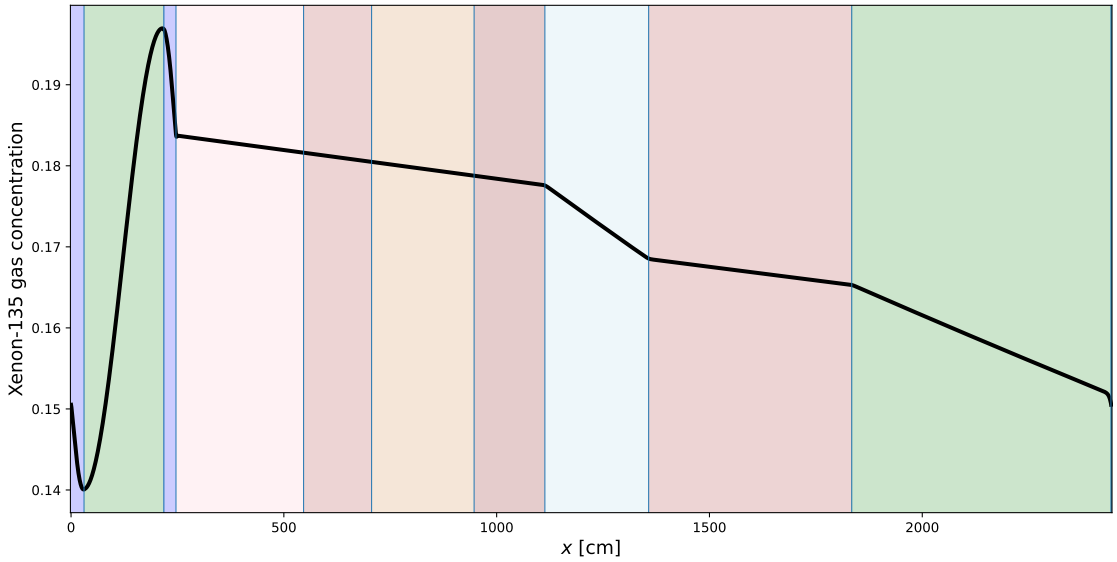

Figure 18. Xenon gas concentration distribution of MSRE 1D loop.

7. DEMONSTRATION OF OFF-GAS SYSTEM FOR NOBLE GASES IN MSRE

The one-dimensional structure of MSRE is designed such that $Q = uA$, where Q represents the volume flow rate, u denotes the liquid velocity, and A stands for the cross-sectional area. This configuration is specifically tailored for operation at 1200 gpm in MSRE in Figure 19. The temperature of the MSRE is obtained from Engel and Haubenreich (1962) [16]. The average reactor temperature is (noted as $_p$ in the primary loop.)

$$T_{\text{reactor}} = T_{p,\text{inlet}} + 0.762\left(T_{p,\text{outlet}} - T_{p,\text{inlet}}\right) \tag{38}$$

The heat exchanger temperature is

$$T_{\text{HX}} = T_{p,\text{inlet}} + 0.5\left(T_{p,\text{outlet}} - T_{p,\text{inlet}}\right) \tag{39}$$

The temperature of the MSRE is essential for determining density, viscosity, and various other parameters as shown in Figure 20. The dimensionless parameters dependent on temperature for these fluid properties are illustrated in Figure 21.

When $k_l \ll k_g/H$ from equation 21, the liquid mass transfer coefficient distributions are depicted in Figure 22, denoted as $K_L = k_l$, representing the liquid overall mass transfer coefficient. On the other hand, the overall gas mass transfer coefficient is related to $K_G = k_l H$, where H is Henry's gas constant.

When analyzing the situation where a mole of noble gas dissolves in a molten salt fluid at a constant temperature, T, the Gibbs free energy equation for K_H in terms of r, T, $\gamma(T)$,α, β, and K_H^0 yields the following expression:

$$K_H(r, T; \gamma(T), \alpha, \beta, K_H^0) = \exp\left(\frac{\Delta G}{RT}\right) \tag{40}$$

The overall change in the Gibbs free energy ($\Delta G = \Delta G_\gamma + \Delta G_v$) of a component system can encompass contributions from both surface and volume energies, as expressed by the following equation:

$$\Delta G(r, T; \gamma(T), \alpha, \beta) = RT \ln(K_H) = 4\pi r^2 \alpha \gamma(T) + \frac{4}{3}\pi r^3 \beta RT, \tag{41}$$

where R is the ideal gas constant, r is the van der Waals radius in angstrom units, and T is the temperature in K. The surface tension of a liquid salt decreases linearly with temperature change at constant pressure, and this behavior can be described using a specific expression for $\gamma(T)$, represented by

$$\gamma(T) = \frac{\partial \gamma(T)}{\partial T}(T - 273.15) + \gamma_0. \tag{42}$$

The change in Gibbs free energy in 2LiF-BeF_2 system has been amended to include the appropriate correction for Henry's gas constant. This corrected equation is then utilized in a nonlinear regression approach that takes into account both the surface and volume energy terms of the Gibbs energy. Equation (41) considers temperature variations and the van der Waals radii of noble gases. The measured solubilities of neon, argon, and xenon gases play a crucial role as input data points for generating the regressed parameters. By employing nonlinear regression analysis with the entirety of this data, it was possible to predict helium and krypton values' solubilities in 2LiF-BeF_2. Additionally, the analysis allowed for the prediction of helium, krypton, and xenon in LiF-NaF-KF. These projections give clearly defined α and β

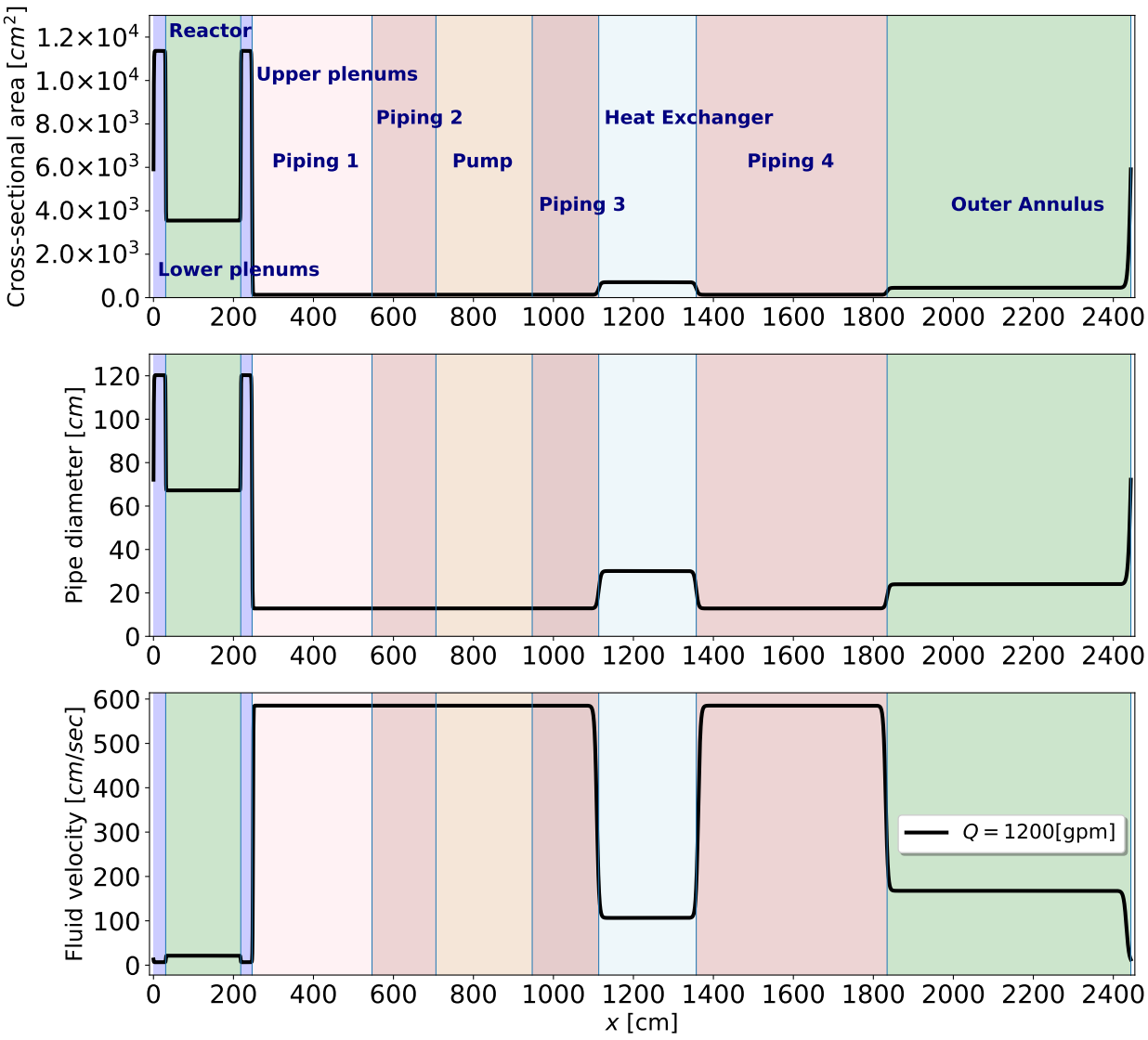

Figure 19. Fluid velocity, cross-sectional area, and pipe diameter distributions of MSRE loop.

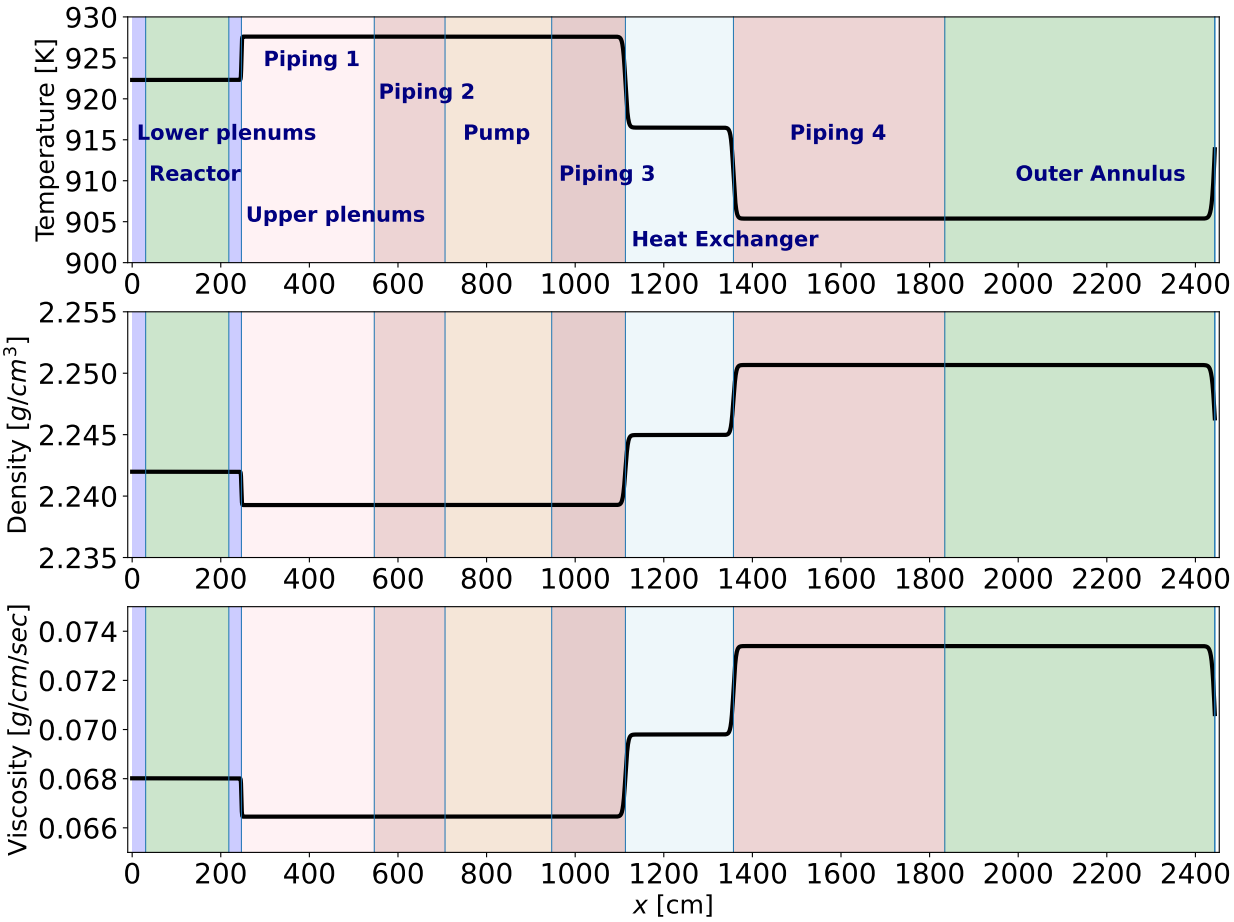

Figure 20. Temperature, density, and viscosity distributions of MSRE loop.

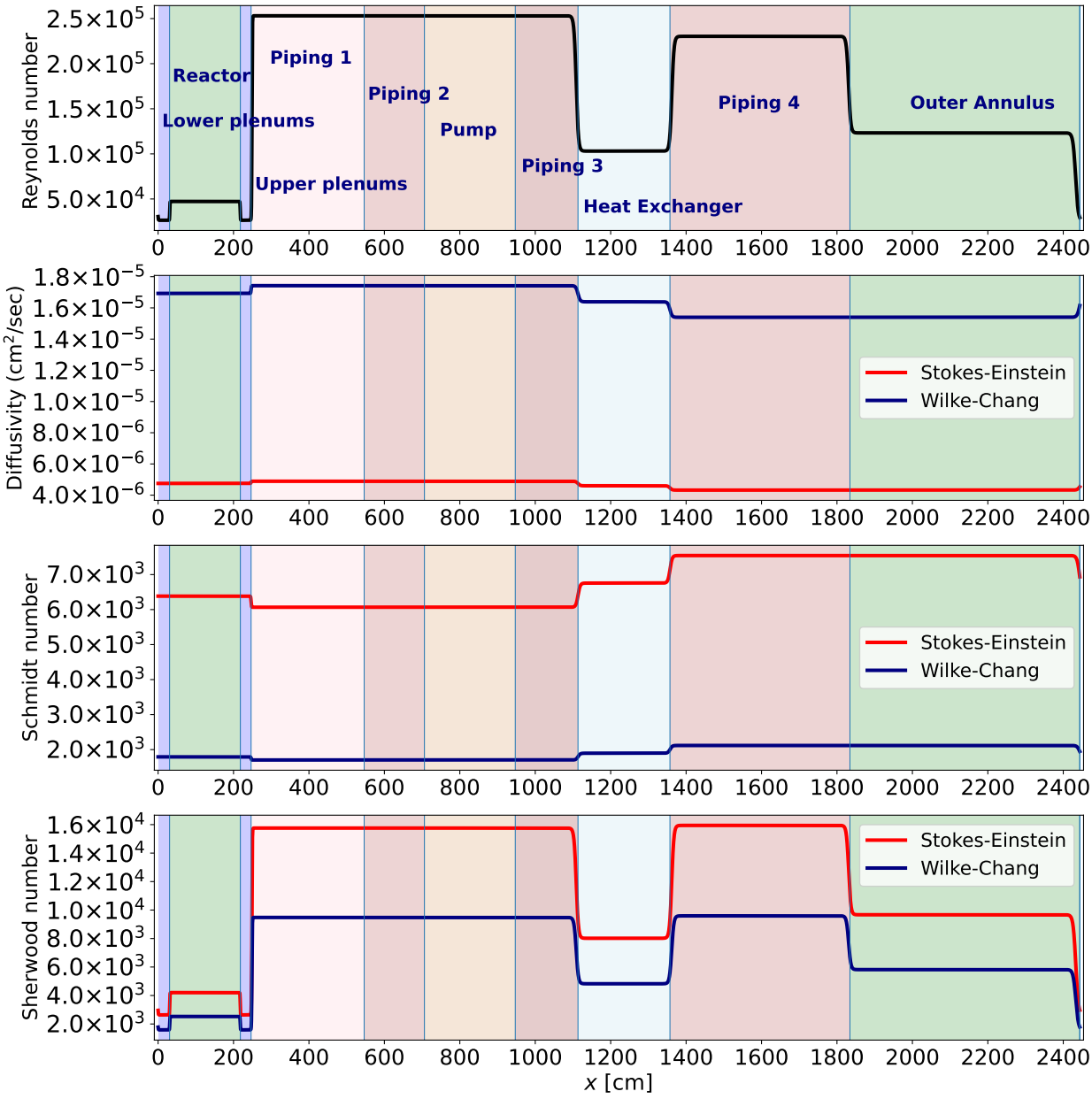

Figure 21. Reynolds number, diffusivity, Schmidt number, and Sherwood number distribution of the MSRE loop related to the Stokes–Einstein and Wilke–Chang theories.

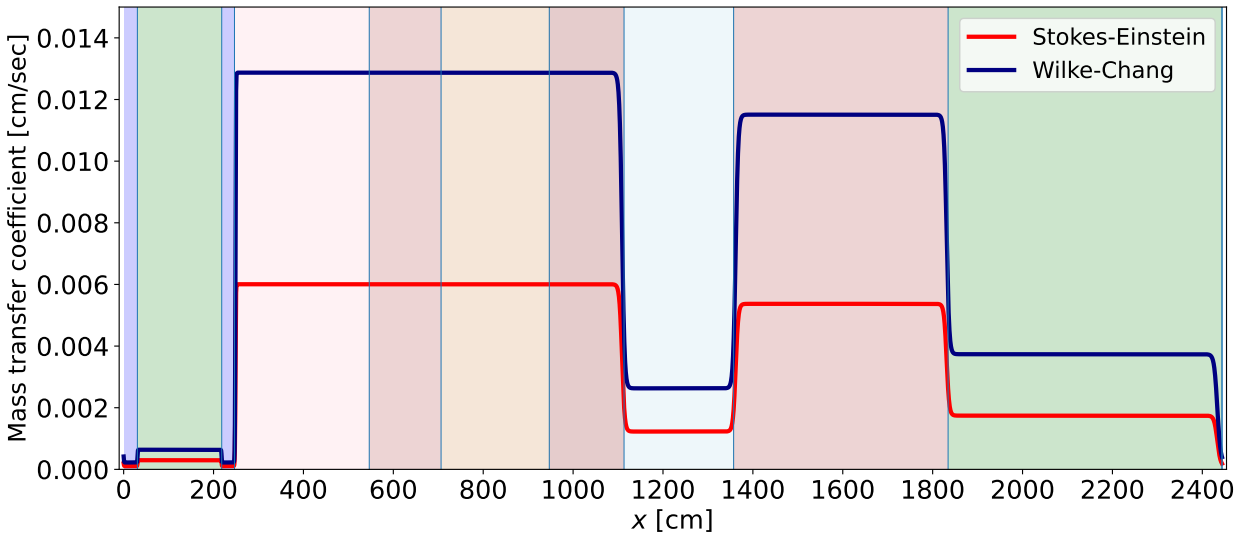

Figure 22. Liquid mass transfer coefficient distributions of the MSRE loop.

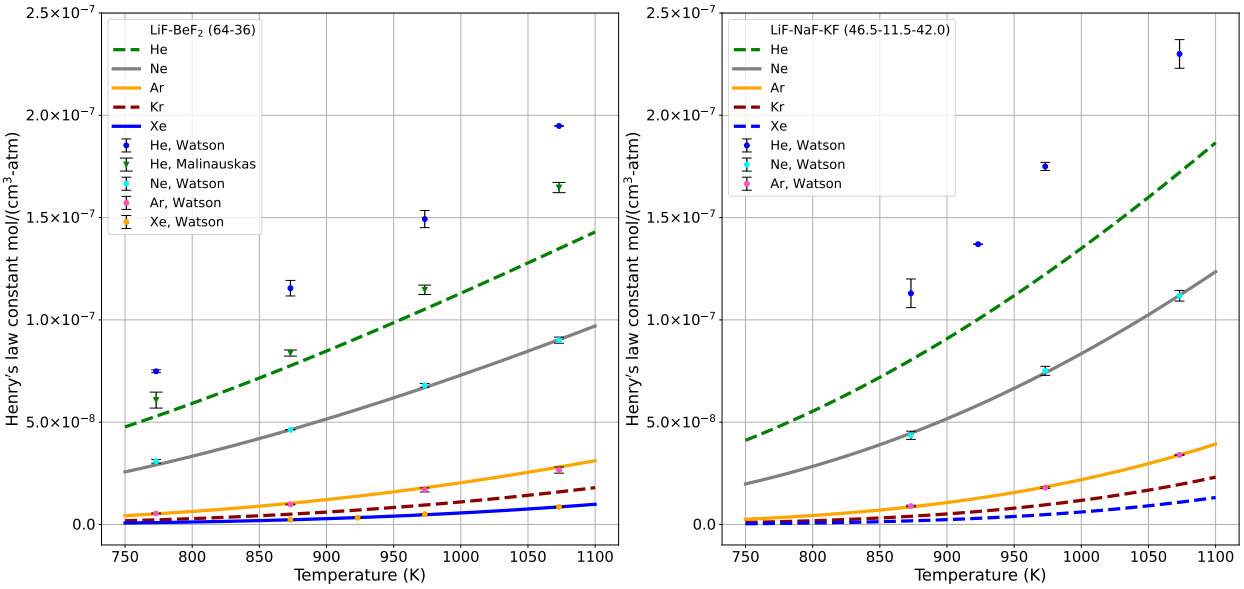

Figure 23. Henry's gas constant for the two salts analyzed, 2LiF-BeF_2 (left) and LiF-NaF-KF (right). [2]

parameters that are inherent to 2LiF-BeF_2 and LiF-NaF-KF salts given in Table 6. The plots of 2LiF-BeF_2 and LiF-NaF-KF salts are presented in Figure **??**

Henry's gas constant in the MSRE loop is depicted with respect to MSRE temperatures in Figure 24 (left). Additionally, the mass transfer coefficient from the fuel salt to the circulating bubbles in Figure 24 (right) is expressed as [14],

$$k^b = 0.089 \frac{D}{L} \mathrm{Re}^{0.69} \mathrm{Sc}^{0.33}. \tag{43}$$

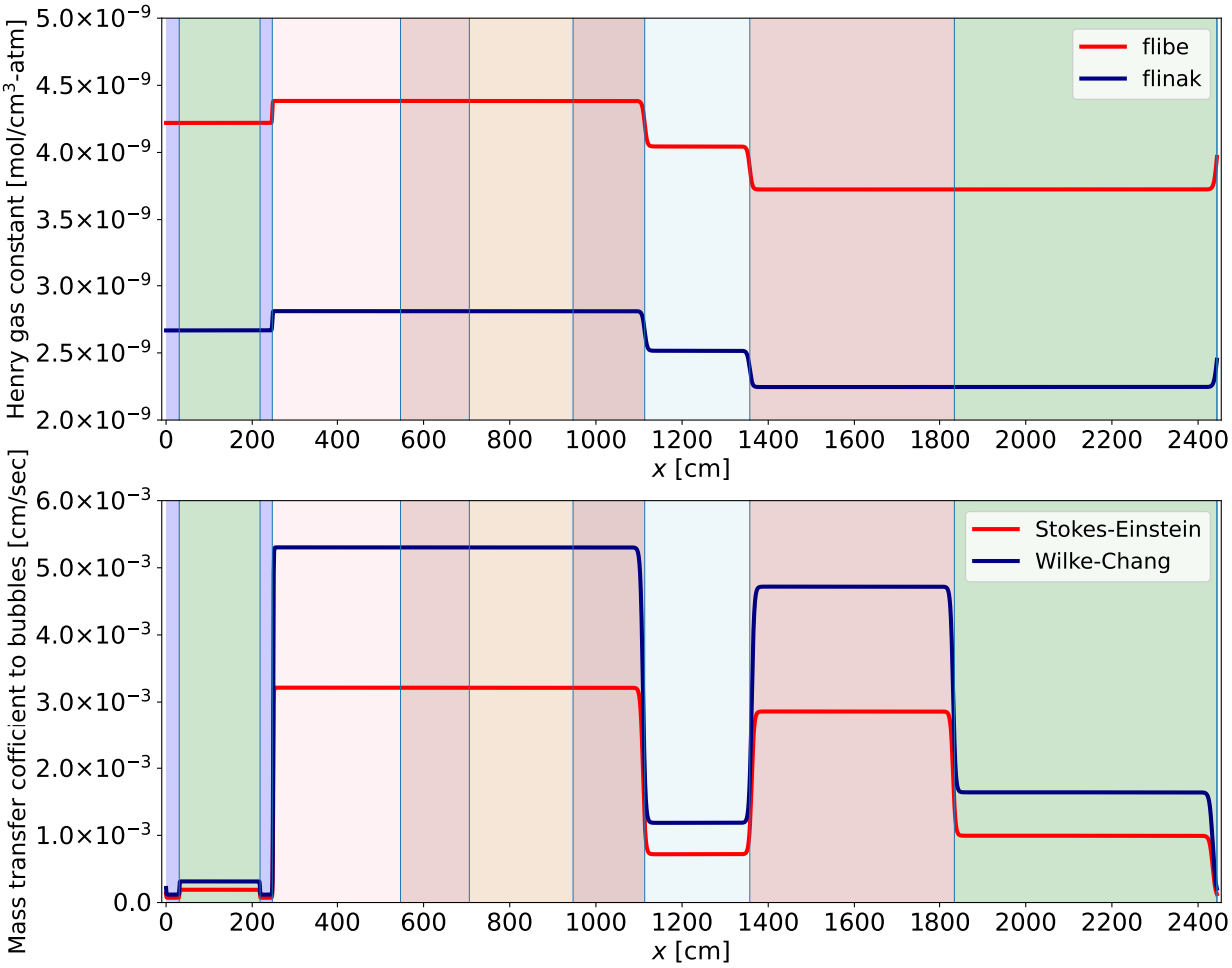

Figure 24. Henry's gas constant and bubbles' mass transfer coefficient distributions of MSRE loop.

The gas velocity is derived from the turbulence relations,

$$u_x^g = u_x^l \left(1 + 2 \sqrt{\frac{0.046 \mathrm{Re}^{-0.2}}{2}} \right) \tag{44}$$

The gas and liquid velocity is presented in the Figure 25

Table 6. The regression model's parameters, including R-squared and reduced chi-square and surface tension [erg/cm^2] **(ref. [17]) are presented. The reduced chi-squared value is obtained by dividing the chi-squared value by the degrees of freedom (ν).**

Parameter	2LiF-BeF_2	LiF-NaF-KF
R^2	0.9988	0.9841
χ^2_ν	144.2	162.4
α	-3.3584 ± 0.0645	-4.6541 ± 0.0938
β	-0.0215 ± 0.0016	0.0105 ± 0.0023
K^0_H	$7.8622\times10^{-7} \pm 0.2190 \times10^{-7}$	$1.4246 \times10^{-6} \pm 0.0644 \times10^{-6}$
Equation (42)	2LiF-BeF_2	LiF-NaF-KF
$\partial\gamma(T)/\partial T$	-0.09	-0.0788
γ_0	235.5	237.0

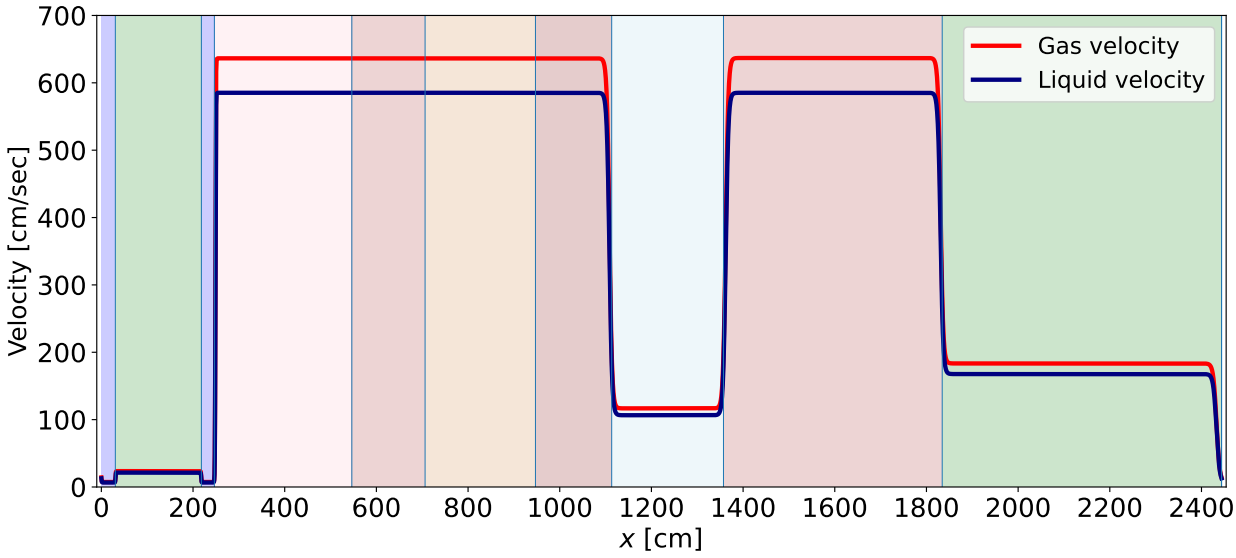

Figure 25. Bubble gas and liquid velocities distributions of the MSRE loop.

The interface mechanism of mass transfer between phases with advection has been considered, and the overall mass transfer coefficients are defined as follows when $k_l \ll k_g/H$ from equation 21:

$$c_l^* = p_g^* H = c_g HRT, \tag{45}$$

$$K_G = K_L H, \tag{46}$$

where noble gases generally follow the ideal gas law; $p_g^* = c_g RT$, in which p_g represents the partial pressure of the species in the gas phase; $R = 82.05746(cm^3 \cdot \text{atm})/(\text{K} \cdot \text{mol})$; and H, Henry's law constant, can also be expressed in the unit mol/(cm$^3 \cdot$ atm).

The gas phase transport does not include an activation term, $\gamma \Sigma_f \phi$, because it is hypothesized that neutron-induced nuclear fission products and iodine decay transition from the liquid phase to the gas phase. When nuclear fission occurs within liquid salts, as in certain types of nuclear reactors, the resulting fission products may initially be dispersed within the liquid phase. However, their progression to the gas phase depends on factors such as volatility and solubility in the liquid phase. Noble gases, for example, tend to shift to the gas phase due to their high volatility and low solubility. This phenomenon is particularly significant in scenarios where the liquid medium undergoes vaporization, as volatile fission products can be carried along in the gas phase. The concentration of the xenon liquid phase is produced from the decay of the parent iodine liquid phase and the activation of the reactor. The concentration of the xenon gas phase originates from the xenon liquid phase.

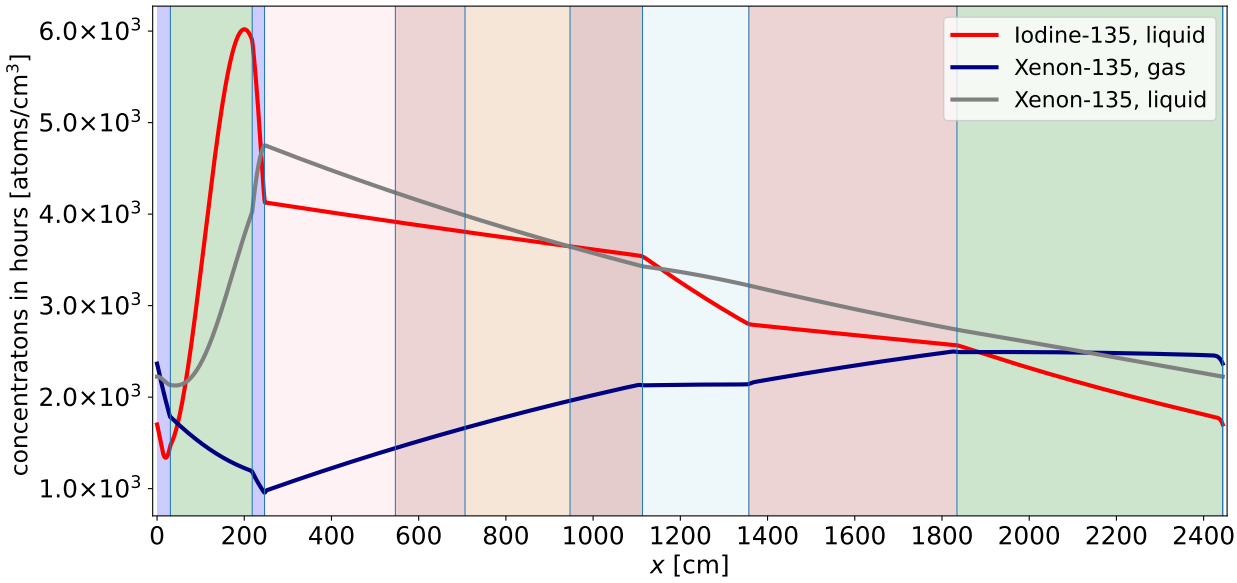

Figure 26. Concentrations of xenon gas and liquid phases from the iodine liquid of the MSRE loop, showing the interfacial area (0.01 [cm^{-1}]) without the off-gas system.

The overall mass-transfer coefficients for the mechanism of steady-state are defined by [18]

$$K_L a\left(c_g HRT - c_l\right) = -K_G a\left(\frac{c_l}{H} - c_g RT\right). \tag{47}$$

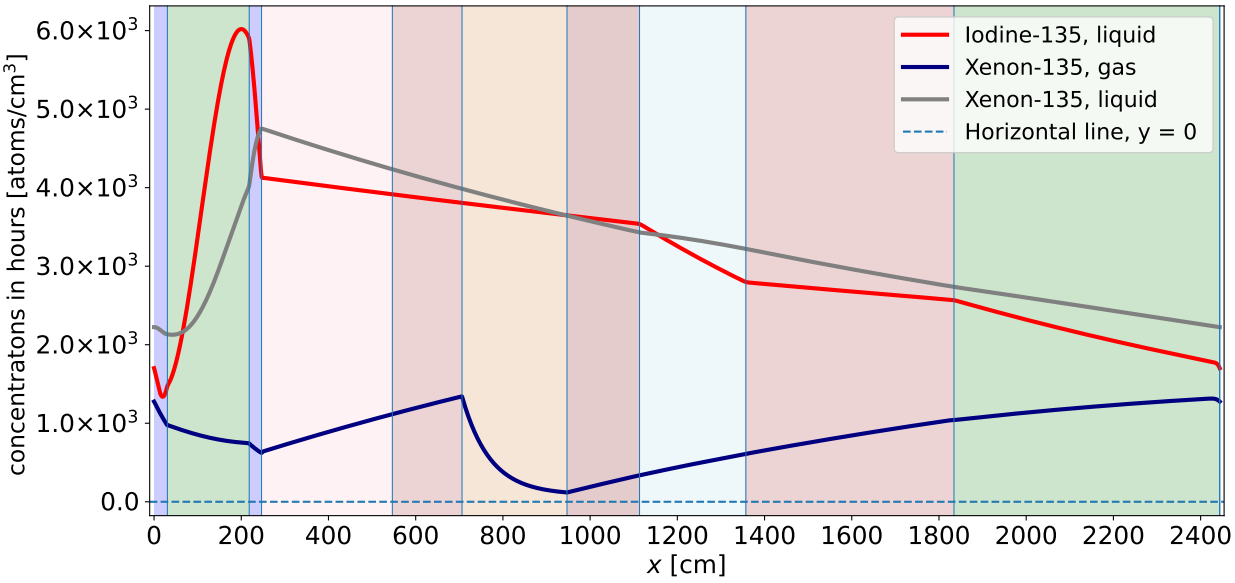

Figure 27. Concentrations of xenon gas and liquid phases from the iodine liquid of the MSRE loop, showing the interfacial area (0.01 [cm^{-1}]) with the off-gas system at pump rate (10 [hr^{-1}]) .

The equations governing mass transport in the liquid and gas phases for concentrations are as follows.

Liquid Phase Transport:

$$A\frac{\partial c_l}{\partial t} + Au_x^l\frac{\partial c_l}{\partial x} = A\gamma\Sigma_f\phi + AK_La\left(c_gHRT - c_l\right) - A\lambda c_l + A\lambda_p c_p \tag{48}$$

Gas Phase Transport:

$$A\frac{\partial c_g}{\partial t} + Au_x^g\frac{\partial c_g}{\partial x} = AK_Ga\left(\frac{c_l}{H} - c_gRT\right) - A\lambda c_g - Amc_g \tag{49}$$

where

- c_l and c_g represent the concentration of the species in the liquid and gas phases, respectively.
- λ and λ_p represent the decay constants of the species (both liquid and gas) and c_p (precursor), respectively.
- u_x^l and u_x^g represent the velocity of the species in the liquid and gas phases, respectively.
- a presents the gas–liquid interfacial area per unit volume.
- K_L and K_G represent the overall mass transfer coefficients in the liquid and gas phases, respectively.
- R represents the universal gas constant.
- m represents the off-gas rate [hr^{-1}] at pump.

Figures 16–18 use constant liquid (or gas) mass transfer coefficients for xenon in both liquid and gas phases. However, Figure 26 uses the automatically generated overall liquid (or gas) mass transfer coefficients, which are based on temperature and other local parameters such as Reynolds number, Schmidt number, etc. Additionally, Figure 27 demonstrates the use of the off-gas system in the pump area (10 hr^{-1} rate).

8. MULTIPHYSICS COUPLING

The various physics of MSRs are highly interconnected and should not be decoupled. Thus, the mass transport equations developed in this work are best used when coupling Mole with other codes. The standalone calculations presented here are merely a demonstration of the methods development and are not actually the recommended way to model an MSR.

The first type of code that Mole should be coupled with is a thermodynamics code such as Thermochimica [19]. Thermochimica takes temperature, pressure, and elemental concentrations as input and performs a Gibbs energy minimization (GEM) calculation. The results of the GEM calculation include the equilibrium chemical potentials and phases of the species in the salt. Though the GEM calculation is by definition an equilibrium calculation, it is expected to be applicable to flowing salt in an MSR because the conditions change gradually throughout the loop and the temperatures are relatively high, so it is expected that the thermodynamics of the salt at a given location will essentially always be at equilibrium for the conditions at that location. Because the Henry's law constants, and thus the mass transfer coefficients, are different for each species in the salt, coupling with a code like Thermochimica is crucial to properly apply the mass transfer coefficients developed in this report. The development of thermodynamics data from the MSTDB-TC [20] by Thermochimica for use in Mole is analogous to the generation of a multigroup cross section library from continuous energy cross sections for use in a deterministic neutron transport code. The coupling with Thermochimica is a one-way coupling; the Mole results are not provided back to Thermochimica and do not influence the Thermochimica calculation in any way.

The second code that Mole should be coupled with is a thermal fluids (TF) code such as SAM or Pronghorn. The TF code calculates fluid velocity, temperature, pressure, and other bulk quantities throughout the MSR loop. The pressure and temperature are necessary for the Thermochimica calculation. The temperature and velocity are necessary for the mass transfer coefficient calculations as shown by equations 40 and 5–15. The results of the Mole calculation will determine how quickly species are moving from the salt to surfaces or gas bubbles and could therefore impact the the density and other properties of the salt; therefore, the coupling between Mole and the TF code is two-way because the results of each code provide feedback to the other code. It should be noted that the TF code should make use of the MSTDB-TP [21] to obtain salt thermophysical properties such as surface tension, viscosity, and density as functions of temperature and pressure. Many of these data are also needed by Mole, so they could be provided to Mole either through the TF code or directly from the MSTDB-TP.

The final crucial piece of the multiphysics coupling is the neutron transport code, such as Griffin. The neutron flux transmutes nuclides in the reactor system; when a nuclide is transmuted from one element to another, the chemistry changes to that of the resulting element. Thus, updated elemental concentrations must be provided to Mole by Griffin; an alternative is that the neutron flux and cross sections are provided to Mole so that it can perform its own transmutation. The latter would be necessary in the event that the chemistry changes are very tightly coupled with the transmutation, but this is not expected to be the case. Figures 26 and 27 demonstrate some aspects of the concentration dependence of various parameters

required for the mass transfer coefficients. Additionally, transfer of any species in the salt to other components or phases affects the cross sections via the addition or removal of particular isotopes, so the results of the Mole calculations are a feedback to the neutron transport calculations. Thus, the Mole and Griffin coupling should also be a two-way coupling. Of course, there is also two-way coupling between the neutron transport and TF that will not be discussed in detail in this report.

This summarizes the multiphysics coupling required for MSR simulation. While Mole is intended to address chemistry phenomena occurring in the reactor, those phenomena are coupled to more traditional reactor physics handled by other codes. Therefore, standalone Mole calculations are unlikely to be useful in practice, and the code should be coupled to other physics tools.

9. REFERENCES

[1] PN Haubenreich, JR Engel, BE Prince, and HC Claiborne. Msre design and operations report. part iii. nuclear analysis. Technical report, Oak Ridge National Lab., Tenn., 1964.

[2] Kyoung O Lee, Wesley C Williams, Joanna McFarlane, David Kropaczek, and Dane De Wet. Semi-empirical model for henry's law constant of noble gases in molten salts. *Scientific Reports*, 14(1):12847, 2024.

[3] Kyoung O Lee, Matthew A Jessee, Aaron M Graham, and David J Kropaczek. Coupled neutronics and species transport simulation of the molten salt reactor experiment. *Nuclear Engineering and Design*, 417:112824, 2024.

[4] Kyoung Lee, Matthew Jessee, Benjamin Collins, Zack Taylor, and Aaron Graham. Transient convective delayed neutron precursors of 235u for the molten salt reactor experiment. Technical report, Oak Ridge National Lab.(ORNL), Oak Ridge, TN (United States), 2022.

[5] Kyoung Lee, Matthew Jessee, Aaron Graham, and David Kropaczek. Coupled neutronics and species transport simulation of the molten salt reactor experiment. *Available at SSRN 4415792*.

[6] Jaakko Leppänen et al. Serpent–a continuous-energy monte carlo reactor physics burnup calculation code. *VTT Technical Research Centre of Finland*, 4, 2013.

[7] James Welty, Gregory L Rorrer, and David G Foster. *Fundamentals of momentum, heat, and mass transfer*. John Wiley & Sons, 2020.

[8] CR Wilke and Pin Chang. Correlation of diffusion coefficients in dilute solutions. *AIChE journal*, 1(2):264–270, 1955.

[9] EL Compere, SS Kirslis, EG Bohlmann, FF Blankenship, and WR Grimes. Fission product behavior in the molten salt reactor experiment. Technical report, Oak Ridge National Lab., Tenn.(USA), 1975.

[10] Kyoung Lee and Matthew Jessee. Multiphysics mass accountancy calculation for noble metals tracking in msre loop. Technical report, Oak Ridge National Lab.(ORNL), Oak Ridge, TN (United States), 2023.

[11] FN Peebles. Removal of *sup*135 xe from circulating fuel salt of the msbr by mass transfer to helium bubbles. Technical report, Oak Ridge National Lab.(ORNL), Oak Ridge, TN (United States), 1968.

[12] JO Hinze. Turbulence 7 an introduction to its mechanism ànd theory, 1959.

[13] Yemada Taitel and Abe E Dukler. A model for predicting flow regime transitions in horizontal and near horizontal gas-liquid flow. *AIChE journal*, 22(1):47–55, 1976.

[14] MW Rosenthal, RB Briggs, and PR Kasten. Molten salt reactor program semiannual progress report for period ending august 31, 1968, ornl-4344, p, 1969.

[15] JR Hightower Jr. Process technology for the molten-salt reactor 233 u–th cycle. Technical report, Oak Ridge National Lab., 1975.

[16] JR Engel and PN Haubenreich. Temperatures in the msre core during steady-state power operation. Technical report, Oak Ridge National Lab.(ORNL), Oak Ridge, TN (United States), 1962.

[17] GM Watson, RB Evans III, WR Grimes, and NV Smith. Solubility of noble gases in molten fluorides. in lif-bef2. *Journal of Chemical and Engineering Data*, 7(2):285–287, 1962.

[18] James Welty, Gregory L Rorrer, and David G Foster. *Fundamentals of momentum, heat, and mass transfer*. John Wiley & Sons, 2014.

[19] M. H. A. Piro et al. The theromchemistry library thermochimica. *Comput. Mater. Sci.*, 67:266–272, 2013.

[20] J. C. Ard et al. Development of the *Molten Salt Thermal Properties Database - Theromchemical (MSTDB-TC)*, example applications, and licl-rbcl and uf3-uf4 system assessments. *J. Nucl. Mater.*, 563, 2022.

[21] J. McMurray et al. Multi-physics simulations for molten salt reactor evaluation: Chemistry modeling and database development. Technical Report ORNL/SPR-2018/864, Oak Ridge National Laboratory, 2018.